Tests on seawater and sea sand concrete-filled CFRP, BFRP and stainless steel tubular stub columns

Y.L. Li[1], X.L. Zhao*[1], R.K. Raman Singh[2, 3] and S. Al-Saadi[2]

[1]Department of Civil Engineering, Monash University, Clayton, Victoria, Australia

(*corresponding author, Email: ZXL@monash.edu)

[2]Department of Mechanical and Aerospace Engineering, Monash University, Clayton, Victoria, Australia

[3]Department of Chemical Engineering, Monash University, Clayton, Victoria, Australia

Abstract:

This paper presents an experimental study on concrete-filled circular tubes that consisted of seawater and sea sand concrete (SWSSC), stainless steel (SS) tube, carbon fibre reinforced polymer (CFRP) tube, and basalt fibre reinforced polymer (BFRP) tube. A total of 38 stub columns, which included 12 hollow section tubes, 12 fully SWSSC-filled tubes and 14 SWSSC-filled double-skin tubes, with four combinations of inner and outer tubes, were tested under axial compression. Tensile coupon tests and "disk-split" tests were conducted to obtain the material properties of SS, CFRP and BFRP. Ultimate strain of SWSSC-filled tubes and stress-strain curves of the confined concrete were characterised in the study. The effects of some key parameters (e.g., tube diameter-to-thickness ratio, cross-section types, outer tube types, and inner tube types) on the confinement effects were also discussed. Comparisons were made among CFRP, BFRP and glass fibre reinforced polymer (GFRP) in terms of confinement to SWSSC. The capacity prediction formulae previously proposed by the authors for SWSSC filled GFRP tubes were found to be reasonable for estimating the load carrying capacity of SWSSC filled CFRP and BFRP tubes.

Keywords: Seawater and sea sand concrete (SWSSC), CFRP, BFRP, GFRP, stainless steel, stub columns, axial compression.

© 2016. This manuscript version is made available under the Elsevier user license
http://www.elsevier.com/open-access/userlicense/1.0/

Nomenclature

A_c	Cross-section area of concrete
A_{cn}	Nominal concrete area
A_i	Cross-section area of inner tube
A_o	Cross-section area of outer tube
A_s	Cross-section area of steel tube
D_i	Diameter of inner tube
D_o	Diameter of outer tube
E_h	Elastic modulus of FRP in hoop direction
E_l	Elastic modulus of FRP in longitudinal direction
E_o	Initial elastic modulus of stainless steel
$\sigma_{0.2}$	0.2% proof stress of stainless steel
f_c	Concrete strength

f_c' Concentric cylinder compressive strength of unconfined concrete

f_{cc}' Confined concrete strength

f_l Confining pressure

f_{scy} Nominal yielding strength of composite sections

f_u Ultimate strength of stainless steel

f_{uh} Ultimate strength in hoop direction of FRP (disk-split test)

f_{ul} Ultimate strength in longitudinal direction of FRP (tensile coupon test)

f_{un} Nominal ultimate strength of composite sections

f_y Yielding strength (= $f_{0.2}$ for SS)

f_{yi} Yielding strength of inner tube

f_{yo} Yielding strength of outer tube

P_p Predicted capacity

P_t Test capacity

t_i Thickness of inner tube

t_o Thickness of outer tube

ε_{cc} Ultimate strain of confined concrete

ε_t Axial strain of hollow sections corresponding to the peak load

ε_{th} Ultimate hoop strain of FRP tube

ε_{tl} Ultimate axial strain

ε_{uh} Ultimate strain of FRP in hoop direction (disk-split test)

ε_{ul} Ultimate strain of FRP in longitudinal direction (tensile coupon test)

γ Void ratio

ν_h Poisson's ratio of FRP in hoop direction

ν_l Poisson's ratio of FRP in longitudinal direction

ζ Confinement factor

σ_c Stress in concrete

σ_t Residual strength of FRP hollow sections

res

(

t Failure stress of hollow sections

1. Introduction

Concrete-filled tubes (CFTs) are being extensively used as the main structural members for resisting axial load in bridge piers and high-rise building columns. The CFT composed of the core concrete and encasing outer tubes is referred as fully concrete-filled tubes in this paper [1]. In order to reduce the self-weight and increase the stiffness, concrete-filled double-skin tubes (CFDST), which consist of an outer and an inner tube with concrete-filled between them, were developed in recent decades [2, 3]. As the core concrete is confined by the encasing tubes and the buckling of the tubes is delayed by the infilled concrete, CFTs and CFDST exhibit greater load-carrying capacities and ductility in comparison with unfilled tubes or plain concrete.

The seawater and sea sand concrete (SWSSC), that utilizes alkali-activated slag as binding material and sea sand as fine aggregate, was investigated in the present study with a view to replacing the conventional ordinary Portland cement (OPC)-based concrete that will avoid the consumption of fresh water, river sand and OPC. Existing literature [4, 5, 6] suggests that the use of geo-polymer (e.g. slag) can considerably reduce the expansion caused by alkali silica reaction (ASR), whereas the mechanical properties of SWSSC is similar to those of conventional Portland concrete. However, the chloride ions in SWSSC can rapidly corrode the carbon steel. Therefore, the corrosion resistant materials (i.e., stainless steel and fibre reinforced polymer) have been investigated in this study.

Stainless steel (SS) has no obvious yield point with considerable strain hardening. Past researches [7, 8] on fully concrete-filled stainless steel tubular columns have demonstrated their desirable structural performance (e.g. greater capacity and ductility) and indicated the current design method for concrete-filled carbon steel tubes to be conservative. However, very little studies are reported on concrete-filled double-skin SS tubes.

The increase demand of the use of fibre reinforced polymers (FRPs) in civil engineering applications is due to their favourable strength to weight ratio and high corrosion resistance. Among

different types of FRPs, glass fibre reinforced polymers (GFRPs) are already widely used in civil engineering. It is well known that the carbon fibre reinforced polymers (CFRPs) have much higher strength and elastic modulus than GFRPs and the basalt fibre reinforced polymers (BFRPs) have similar mechanical properties to GFRPs for the similar fibre volume fractions [9, 10]. Many studies [11, 12, 13] have been conducted on concrete-filled FRP wraps (with fibre exclusively oriented in hoop direction) as an important approach for strengthening existing structures. Prof. J.G. Teng of The Hong Kong Polytechnic University proposed the use of seawater and sea sand concrete with FRP to construct marine/coastal structures [14] and later promoted it internationally [15]. In recent years, researchers [16, 17] have started to apply concrete-filled GFRP tubes (with glass fibres oriented both in hoop and longitudinal directions) in new constructions since the GFRP tube can be used as permanent formwork. The authors of this paper have recently reported performance of SWSSC-filled GFRP tubes [18]. To the best of authors' knowledge, there are no experimental studies on SWSSC-filled CFRP or BFRP tubes.

This paper presents an experimental study on concrete-filled circular tubular stub columns made of seawater and sea sand concrete (SWSSC), stainless steel (SS) tube, carbon fibre reinforced polymer (CFRP) tube or basalt fibre reinforced polymer (BFRP) tube. Both the fully concrete-filled tubes and concrete-filled double-skin tubes were tested under axial compression. The SWSSC mixture developed by the authors [18] was adopted in this testing program. The material properties of SWSSC, SS, CFRP and BFRP were obtained by standard testing methods. The load sharing of core concrete and encasing tubes as well as confinement effect provided by three types of FRPs were investigated. Finally, a unified approach was adopted to predict the load carrying capacity of SWSSC-filled SS, BFRP, CFRP and GFRP tubes in compression.

2. Experimental Program

2.1 Specimen

A total of 38 circular stub columns, including 12 hollow section tubes, 12 fully SWSSC-filled tubes, and 14 SWSSC-filled double-skin tubes, were prepared and tested in the present study. Four different tube dimensions (i.e. with nominal tube diameter of 50 mm, 101 mm, 114 mm and 165 mm, and nominal tube thickness of 3 mm) were selected. In order to eliminate the influence of global buckling and end effects, the length of fully SWSSC-filled tubes with outer dimeter of 50 mm (i.e. S50-H, C50-H, B50-H, S50-C, C50-C, and B50-C) was 150 mm and the length of all the other specimens was 400 mm.

The cross-section configuration of the specimens is illustrated in Fig. 1 and the measured dimensions of the specimens are listed in Table 1, in which the concrete strength (f_c') and failure loads (N_t) are also included. The label of the specimen consists of the outer tube material ("S" for stainless steel, "C" for CFRP and "B" for BFRP) followed by outer tube nominal diameter ("50", "101", "114", and "165"), inner tube material followed by inner tube nominal diameter (if applicable), and cross-section type indicator ("H" for hollow sections and "C" for SWSSC-filled tubes). For example, S50-C refers to fully SWSSC-filled SS tubes with D_o of 50 mm, and S114-B50-C refers to SWSSC-filled double skin tubes with an SS outer tube (D_o = 114 mm) and BFRP inner tube (D_i = 50 mm). A similar labelling system was adopted in [18] where the letter "F" defined the GFRP filled tubes. However, in this current paper more specific identifications have been used. Accordingly, letters "C", "B" and "G" have been incorporated into the labels to represent CFRP, BFRP and GFRP respectively. For example, specimen "S114-F50-C" is now called "S114-G50-C", which refers to SWSSC-filled double skin tubes with an SS outer tube (D_o = 114 mm) and GFRP inner tube (D_i = 50 mm).

2.2 Material properties

2.2.1 Seawater and sea sand concrete (SWSSC)

A proper SWSSC mix was developed by the authors [18] to achieve the target strength and desirable workability with the slump of fresh concrete reaching 160 mm. The same concrete mix developed in [18] was adopted in this study. The mix includes: slag (360 kg/m^3), seawater (190 kg/m^3), sea sand (830 kg/m^3), coarse aggregate (1130 kg/m^3), hydrate lime slurry (14.4 kg/m^3) and sodium metasilcate (38.4 kg/m^3) as activator. More details of the SWSSC can be found in [18].

Three batches of concrete were cast and three identical standard cylinders (with diameter of 100 mm and height of 200 mm) were prepared for each batch in order to measure the concrete strength (f_c'). All the specimens and cylinders were sealed by plastic film to avoid the moisture evaporation and aged to 28 days. The concrete strength (f_c') is listed in Table 1, which varies from 32.8 MPa to 39.4 MPa.

2.2.2 Stainless steel

The SS tubes were made of 316 grade austenitic stainless steel in accordance with AS/NZS 4673 [19]. Three tensile coupons were cut from each size of SS tube and the ends of the coupons were flattened in order to be gripped by test machine. The tensile coupon test was conducted according to AS 1391 [20] with a loading rate of 1 mm/min. The averaged proof stress ($f_{0.2}$) and ultimate tensile strength (f_u) are summarised in Table 2. A typical stress-strain curve for stainless steel is plotted in Fig. 2, in which the full range strain was obtained from laser-extensometer (gage length = 50 mm), the initial range strain was obtained from strain gauges attached at the middle part of coupons and the initial elastic modulus (E_o) is 195 GPa.

2.2.3 Carbon fibre reinforced polymer (CFRP) and basalt fibre reinforced polymer (BFRP)

The CFRP and BFRP tubes were fabricated by filament winding process with epoxy as the matrix. Based on the data provided by the manufacture, the fibre-volume fraction is about 60%. In order to provide strength and stiffness in both longitudinal and hoop directions, the fibres were

oriented in different directions and 20%, 40%, and 40% fibres were in the angle of 15°, ±40°, and ±75° with respect to the longitudinal axis of tubes. The same orientation was used for manufacturing GFRP tubes reported in [18].

The material properties of CFRP and BFRP in the longitudinal direction were obtained by tensile coupon test. Three coupons were cut from each size of tubes. Two pairs of grippings were attached on the coupon ends to ensure proper gripping. The tensile test was conducted in accordance with ASTM D3039 [21] with a loading rate of 0.5 mm/min. The material properties in the hoop direction were obtained by the "disk-split" test specified in ASTM D2290 [22] with a loading rate of 0.5 mm/min. Three 20 mm wide rings were cut from each size of tubes for "disk-split" test. Details of the test setup can be found in [18].

A summary of the test results is reported in Table 3, in which f_{ul}, ε_{ul}, E_l, and ν_l is the ultimate strength, ultimate strain, elastic modulus, and Poisson's ratio in longitudinal direction, whereas f_{uh}, ε_{uh}, E_h, and ν_h is the ultimate strength, ultimate strain, elastic modulus, and Poisson's ratio in hoop direction. The strain was the averaged strain gauge readings and the elastic moduli were calculated in accordance with ASTM D3039 [21]. The data for GFRP (with similar fibre volume fraction and fibre orientations) in [18] is also listed in Table 3.

Since the same manufacture process, fibre volume fraction and fibre orientations were used for different tube sizes, there is no significant difference in material properties between tubes with different diameters, which is also demonstrated in Table 3. In the following discussion, the influence of tube diameter is ignored and material properties of CFRP or GFRP is taken as the averaged value of all the tubes. As shown in Table 3, the ultimate strength and elastic moduli in hoop direction are much higher than those in the longitudinal direction. The f_{uh} to f_{ul} ratio (f_{uh}/f_{ul}) is 2.4, 2.7, and 1.4 for CFRP, BFRP and GFRP respectively. CFRP has the highest ultimate strength and elastic moduli in both directions, which is in agreement with previous studies [10, 23]. BFRP has the lowest ultimate strength and elastic modulus in longitudinal direction, while the material

properties of BFRP in hoop direction are similar to those of GFRP. With regard to ultimate strain, there is no obvious difference between ultimate strain in longitudinal and hoop directions. The ultimate strain of CFRP is much less than that of BFRP and GFRP. The Poisson's ratio for all the FRPs is about 0.3 except for CFRP in hoop direction, which indicates that the Poisson's ratio does not vary considerably for different type of fibres.

Typical stress-strain curves of CFRP, BFRP and GFRP are plotted in Fig. 3. As shown in Fig. 3, the stress-strain behaviour of FRP in the hoop direction can be regarded as linear. However, the stress-strain behaviour of FRP in the longitudinal direction is not purely linear and some nonlinearity is observed during the stage before failure.

2.3 Test setup

All hollow section tubes were tested using a 500 kN capacity Baldwin machine, whereas all the SWSSC-filled tubes were tested in a 5000 kN capacity Amsler machine. The load was directly applied on the specimen through a loading plate. The cement paste was used to fill the gap caused by the shrinkage of concrete so that the axial load could be simultaneously applied on the core concrete and encasing tubes.

Three linear variable displacement transducers (LVDTs) were placed in an equidistant configuration around the specimens to measure the axial end shortening. Three stain gauges were fixed in the longitudinal direction and another three strain gauges were fixed in the circumferential direction at the mid-height of specimens. More details of the test setup and instrumentations can be found in [18].

The axial strain can be obtained by two approaches: (1) averaged axial end shortening divided by specimen length which is called "axial strain (from LVDT)"; (2) averaged reading of strain gauges in longitudinal direction which is called "axial strain (from strain gauge)". In the following discussion, if without specific noting, the axial strain refers to "axial strain (from LVDT)".

3. Test Results

3.1 Hollow sections

As the length-to-diameter ratio is less than 4 for all the SS hollow section tubes, the specimens failed by yielding and plastic local buckling. The failure modes of the specimens are shown in Fig. 4 where the elephant foot was formed during the late stage of the test. The test results for SS hollow section tubes under axial compression are summarized in Table 4, in which $f_{0.2}$ is 0.2% proof stress of SS, σ_t is the failure stress (equals to the peak load divided by cross-section area), ε_t is the axial strain corresponding to the peak load. As shown in Table 4, with the increase of D_o/t_o, the $\sigma_t/f_{0.2}$ and ε_t decrease since the cross-section becomes more slender. The stress-strain curves of SS hollow sections are plotted in Fig. 5, where obvious strain hardening can be observed. A comparison between Fig. 5 (a) and (b) indicates that when the tube is under large deformation (i.e. after the peak load), the strain obtained from LVDT cannot represent the real strain of the SS tube.

The failure mode of CFRP and BFRP hollow section tubes is local buckling near the ends. The stress-strain curves are plotted in Fig. 6, and a summary of the test results is listed in Table 5. The hollow sections can resist the load linearly until a sudden failure causing a dramatic drop of applied load. Because of the occurrence of local buckling, the compression strength (σ_t) and ultimate strain (ε_t) of hollow tubes generally cannot reach the tensile strength (f_{ul}) and ultimate tensile strain (ε_{ul}) obtained by coupon test. With the increase of D_o/t_o, the σ_t/f_{ul} and ε_t generally decrease slightly but this trend is not as clear as that for SS hollow sections. One possible reason is that the local buckling of FRP is more complicated due to the large number of fibres involved. As shown in Fig. 6, there is no nonlinearity of stress-strain curves for FRP hollow sections under axial compression, which is different from the results of tensile coupon test. The "stiffness" in Table 5 is the slope of stress-strain curves (before reaching the peak load) in Fig. 6. The stiffness (from strain gauges) for CFRP is close to the elastic modulus (E_l), which is as expected. However, the stiffness (from strain gauges) for BFRP is much higher than the E_l. After the occurrence of local buckling, the FRP

hollow section still has some residual strength. In this paper, the residual strength (σ_{res}) is roughly taken as the averaged stress after reaching the peak load, as defined later in Fig. 9(b).

3.2 SWSSC-filled tubes

The load-axial strain curves of SWSSC-filled tubes are classified into three groups (Fig. 7) based on the outer tube material type: (a) SWSSC-filled SS tubes; (b) SWSSC-filled CFRP tubes; (c) SWSSC-filled BFRP tubes. In general, the material type of the outer tube has a greater influence on the behaviour. The strength and ductility of the concrete-filled tubes are substantially enhanced in comparison with the hollow tubes or the plain concrete.

The tests for SWSSC-filled SS tubes were terminated due to the limited stroke of test machine (about 60 mm), and the ultimate capacity (N_t) was taken as the maximum load within 5% axial strain. Similar definition of N_t for concrete-filled SS tubes was also adopted by Lam and Gardner [7]. The ultimate capacity (N_t) for SWSSC-filled CFRP and BFRP tubes is taken as the maximum load the specimen can sustain during the test. The ultimate capacity of all the specimens is listed in Table 1.

Obvious strain hardening behaviour is observed for fully SWSSC-filled SS tubes (Fig. 8 (a)). When SS is used as both outer and inner tubes (Fig. 8(b)), the shape of load-axial strain curves of specimen S114-S50-C is similar to that of S165-S114-C but there is an obvious drop of applied load for specimen S165-S101-C with a more slender inner tube. For double-skin tubes with SS as the outer tube and CFRP/BFRP as the inner tube (Fig. 8 (c)), there is a sudden drop of applied load caused by the buckling of inner FRP tube that was accompanied by a loud noise. Fig. 8 (b, c) indicates that the amplitude of the load drop mainly depends on the diameter-to-thickness ratio (D_o/t_o), void ratio (D_i/D_o) and inner tube type. In general, the SWSSC-filled SS tubes (both fully filled and double-skin tubes) exhibit high ductility. The failure mode was a folding failure mechanism (yielding and local buckling), which is in agreement with the observation of other researchers [7, 8].

Obvious bilinear response was observed for SWSSC-filled CFRP and BFRP tubes (Fig. 8 (d-g)), which is different from the load-strain curves of SWSSC-filled SS tubes. The failure mode for SWSSC-filled FRP tube is the outer tube rupture in hoop direction (except specimen C165-C101-C, B114-B50-C, and B165-B101-C). Based on the test observation, the ruptures of the CFRP tubes were more sudden than those of the BFRP tubes. For specimens C165-C101-C, B114-B50-C, and B165-B101-C, local buckling of inner tubes occurred. It seems that slender CFRP and BFRP inner tubes are more susceptible to local buckling. These specimens failed in longitudinal direction (i.e. buckling of tubes and crushing of concrete) before the rupture of the outer tubes. Although the failure mode of these specimens is different from the rest of the SWSSC-filled FRP tubes, their axial strain at failure (around 0.03 to 0.04) is very close to that for other specimens. As shown in Fig. 8 (d-g), slight load drop was observed for the SWSSC-filled FRP specimens before reaching the ultimate capacity, which is caused by the local buckling of the FRP tubes. A comparison between Fig. 8 (d) and (f) indicates that the strength enhancement caused by the CFRP tube is more considerable than the BFRP tube since the hoop strength of the CFRPs is much higher than that of the BFRPs. On the condition that the failure mode is tube rupture, there is not much difference of the shape of load-axial strain curves for fully filled tubes and double-skin tubes.

4. Discussion

4.1 Ultimate strain of CFRP and BFRP tubes

The first buckling strain refers to the axial strain corresponding to the first occurrence of local buckling for the CFRP and BFRP tubes, which can be observed during the test. The first buckling strain for tested specimens is summarized in Table 6, in which “Hollow” refers to the buckling strain of corresponding hollow sections.

Based on Table 6, several conclusions can be made: (1) the strain obtained by LVDTs is larger than that by strain gauges and similar findings were reported by other researchers [18, 24]; (2) the tube diameter-to-thickness ratio does not substantially affect the first buckling strain, which is

different from the case of hollow sections; (3) the first buckling strain is larger than the buckling strain of corresponding hollow sections, indicating the fill-in concrete can delay the buckling of FRP tube; (4) the first buckling strain of other tubes (from strain gauges) is slightly less than the ultimate tensile strain obtain from coupon test (ε_{ul}=0.0088 for CFRP, ε_{ul} =0.0142 for BFRP) due to the local buckling; (5) The first buckling strain of inner tubes is in the same range (0.006 to 0.01) for all three FRPs.

The ultimate axial strains (ε_{tl}, from LVDTs) corresponding to ultimate capacity are listed in Table 7, in which the ultimate tensile strain in longitudinal direction (ε_{ul}) is also provided. The specimens that failed by tube rupture have much higher ultimate axial strain than specimens that failed by tube buckling and concrete crushing (i.e. C165-C101-C, B114-B50-C, and B165-B101-C). Table 7 indicates that with the increase of outer tube diameter-to-thickness ratio (D_o/t_o), the ultimate axial strain generally decreases slightly. The ultimate axial strain is much lower than the material property obtained from tensile coupon test (i.e. ε_{ul}). Even though the tubes failed in the longitudinal direction, the specimen can still increasingly sustain the load as the core concrete is effectively confined by the encasing tubes in hoop direction.

The ultimate hoop strain (ε_{th}) is taken as the averaged readings of strain gauges in hoop direction and the results are summarized in Table 7. As mentioned previously, some double-skin specimens (i.e. C165-C101-C, B114-B50-C, and B165-B101-C) did not fail by tube rupture and the ultimate axial strain is much less than for the other specimens failed by tube rupture. The ultimate hoop strain of concrete-filled CFRP tubes (except specimens without tube rupture) is slightly higher than that obtained from "disk-split" test (ε_{uh}). The ε_{th} of BFRP tubes agrees well with the ε_{uh}, which is similar to the conclusions of GFRP tubes [18]. As shown in Table 7, the outer tube diameter-to-thickness ratio does not obviously affect the hoop rupture strain, and there is no obvious difference in hoop rupture strain between fully filled tubes and double-skin tubes.

4.2 Load distribution

It is well known that the confined concrete strength (f_{cc}') is higher than the unconfined concrete strength (f_c') due to the confinement effect provided by the encasing tubes. In order to discuss the confinement effect, the load resisted by core concrete should be firstly determined.

As both the core concrete and encasing tubes sustain the applied load simultaneously, the load shared by core concrete is calculated by the following criteria: (1) the load carried by concrete is equal to the difference between the applied load and the load carried by tubes at the same axial strain; (2) the load carried by SS tubes can be determined by the simplified model in Fig. 9 (a), in which the axial load-strain curves for corresponding hollow sections were obtained from the tests; (3) the load carried by outer CFRP and BFRP tube is the product of the axial strain (from strain gauges), stiffness (obtained from compression test on hollow sections: 40.0 GPa for CFRP tube and 23.9 GPa for BFRP tube) and cross-section area; (4) the load carried by inner CFRP and BFRP tube is determined by the simplified model in Fig. 9 (b), in which the axial strain is obtained from LVDTs, E is elastic modulus of hollow sections (31.4 GPa for CFRP tube and 18.8 GPa for BFRP tube), f_{ul} is longitudinal strength, ε_l is the first buckling strain (as highlighted in load-strain curves in Fig. 8), σ_{res} is the averaged residual strength (listed in Table 5); (5) the stress in CFRP and BFRP tubes should not exceed the f_{ul} obtained by tensile coupon test.

The criteria in the present paper is similar to the method adopted in [18] except the addition of criterion (5) as an improvement of the method in [18]. The load-distribution curves of the specimens are presented in Fig. 10. The stress in the concrete is estimated as the load carried by concrete divided by cross-section area of concrete. Although the stress-strain curves of concrete are not accurate due to the complexity caused by tube buckling, the relative comparison between specimens is still helpful in understanding the influence of some key parameter on the behaviour of confined concrete as discussed in the followings.

4.3 Concrete confinement

4.3.1 Effects of tube diameter-to-thickness ratio (D_o/t_o)

As shown in Fig. 11 (a), the tube diameter-to-thickness ratio does not significantly affect the σ_c/f_c'-strain curves of fully SWSSC-filled SS tubes. Obvious bilinear stress-strain response is observed for concrete confined by CFRP and BFRP tubes (Fig. 11 (b, c)). With the increase of D_o/t_o, both the confined concrete strength (f_{cc}') and ultimate strain (ε_{cc}) decrease. This is in agreement with existing research on concrete confined by FRP wraps [11], i.e. the increase of D_o/t_o can attribute to a decrease of confining pressure (f_l) on the concrete. A comparison between Fig. 11 (b) and (c) indicates that CFRP tubes with higher hoop strength can provide greater confinement effect on the concrete than the BFRP tubes. Fig. 11(d) compares three types of FRP tubes fully filled with SWSSC. It seems that GFRP and BFRP provide similar confinement, whereas more confinement is achieved by CFRP.

4.3.2 Effects of cross-section types (fully filled and double-skin)

As shown in Fig. 12 (a), compared to fully filled tubes, when the specimen is under large deformation, there is a drop of σ_c/f_c' for double-skin tubes as the inner tube cannot effectively resist the inward expansion of concrete. The amplitude of the load drop and residual strength depend on the void ratio (D_i/D_o), outer tube diameter-to-thickness ratio (D_o/t_o), and inner tube material type. The load drop of double-skin tubes with SS as the outer tube and CFRP/BFRP as the inner tube is more severe due to the buckling of inner FRP tube.

Fig. 12 (b) to Fig. 12 (d) indicate that there is not much difference of σ_c/f_c'-strain curves for double-skin tubes (CFRP or BFRP or GFRP as the outer tube and SS as the inner tube) and corresponding fully filled tubes. The rupture of the outer tube occurs earlier than the occurrence of large deformation of inner SS tube so that the inner tube can effectively resist the inward expansion of concrete. For double skin tubes with FRP as both outer and inner tubes, the behaviour is similar until the slender inner tube (C101 and B101) buckles at an axial strain around 0.03.

4.3.3 Effects of outer tube types

The types of outer tube (SS tube or FRP tube) can obviously affect the shape of σ_c/f_c'-strain curves (Fig. 13). The strength enhancement caused by FRP tube is more significant than that by SS tube, but the strain in SWSSC-filled SS tube is much higher than that in SWSSC-filled FRP tube. Furthermore, the confinement effect by CFRP is greater than that by BFRP or GFRP due to the higher hoop strength of the former (CFRP).

The different shapes of σ_c/f_c'-strain curves for SWSSC-filled SS tubes and SWSSC-filled FRP tubes are substantially attributed by their different material properties. When the lateral expansion of concrete exceeds that of FRP tube, the confining pressure on the concrete increase continually due to the linear stress-strain response of FRP in hoop direction. This kind of confinement effect is called as "passive confinement effect". However, "active confinement effect" occurs in SWSSC-filed SS tubes where confining pressure provided by SS tube slows down after the SS reaches yield strength (0.2 % proof strength).

4.3.4 Effects of inner tube types

In general, the buckling of inner FRP tube can cause a sudden drop of applied load. When the outer tube is SS (Fig. 14 (a)), the influence of inner tube types on the shape of σ_c/f_c'-strain curves is not significant. The residual strength mainly depends on the void ratio (D_i/D_o) and the outer tube diameter-to-thickness ratio (D_o/t_o). It is believed that when the specimen is under large deformation, the inner tube cannot restrain the inward expansion of core concrete.

For specimens with CFRP and BFRP as the outer tube, when the failure mode is tube rupture, the effects of inner tube types can be ignored. However, the inner FRP tubes in some specimens (e.g., C165-C101-C and B165-B101-C with slender inner tubes) cannot effectively restrain the concrete after axial strain reaches around 0.03 and the rupture of the outer FRP tube does not happen. In this case, the concrete strength enhancement caused by confinement effect and the ductility are much less than those of the corresponding double-skin tubes with SS as the inner tube

since the hoop strength of the outer tube is not fully utilized. Fig. 14(d) compares the confinement provided by three types of FRPs. When SS inner tube is used, BFRP and GFRP outer tubes perform at a similar level, but CFRP outer tube provides greater confinement effect. When FRP is used as both inner and outer tubes, BFRP and GFRP have similar behaviour, whereas CFRP achieves greater confinement effect.

5. Capacity Prediction

5.1 Fully SWSSC-filled stainless steel tube

Current design codes do not cover the ultimate capacity of fully concrete-filled SS tubes under axial compression. Past research [7] indicated that the design methods for fully concrete-filled carbon steel tubes is conservative for fully concrete-filled SS tubes. Li et al. [18] made some modifications of a design method for concrete-filled carbon steel tubes, which was proposed by Han et al. [25], and applied it to fully SWSSC-filled SS tubes. The method proposed by Li et al. [18] is adopted to estimate the load carrying capacity of specimens tested in the present study.

The predicted ultimate capacity (N_p) of fully SWSSC-filled SS tubes can be determined by Eqs. (1a) to (1c):

$$N_p = (A_s + A_c) f_{scy} \tag{1a}$$

$$f_{scy} = (1.14 + 1.4\xi) f_c' \tag{1b}$$

$$\xi = \frac{A_s f_y}{A_c f_c'} \tag{1c}$$

where A_s is cross-section area of SS tube, A_c is cross-section area of concrete, f_c' is concrete strength, f_y is yield strength (=$f_{0.2}$ for SS), ξ is confinement factor, and f_{scy} is nominal yield strength of composite sections. In [18], the relationship between f_{scy}/f_c' and ξ (i.e. Eq. (1b)) was determined by the regression analysis of available existing data [7, 8, 18, 26, 27]. The regression analysis is summarized in Fig. 15, in which the test data of the present study is also included and the dashed

line represents the Eq. (1b). It can be seen that the current data are in the same scatter band as the existing data.

A comparison between the experimental capacity and predicted capacity by the method proposed by Li et al. [18] is presented in Table 8. The data in [18] is also included in Table 8. As shown in Table 8, this method slightly over estimate the capacity of fully SWSSC-filled SS tubes, especially for the specimens in the present study. One reason is that the load corresponding to 5% axial strain is adopted as N_t but the applied load can still increase slightly after the axial strain of 5% for some fully SWSSC-filled SS tubes (see Fig. 8(a)). In general, this method can provide reasonable estimation of the ultimate capacity of fully SWSSC-filled SS tubes.

5.2 SWSSC-filled double-skin tubes (SS as the outer tube)

The formulae presented in [18] is adopted herein to estimate the ultimate capacity of SWSSC-filled double-skin tubes (SS as the outer tube). It is assumed in [18] that the capacity of double-skin tubes is the summation of the capacity of outer SS tube with sandwiched concrete (with appropriate modification) and the capacity of inner SS or FRP tube. The detailed formulae can be found in [18]. They are summarised here for the convenience of readers.

$$N_p = (A_o + A_c) f_{scy} + A_i f_{yi} \tag{2a}$$

$$f_{scy} = \frac{\alpha}{1+\alpha} \chi^2 f_{yo} + \frac{1+\alpha_n}{1+\alpha} (1.14 + 1.4\xi) f_c' \tag{2b}$$

$$\xi = \frac{A_o f_{yo}}{A_{cn} f_c'} \tag{2c}$$

$$\alpha = A_o / A_c \tag{2d}$$

$$\alpha_n = A_o / A_{cn} \tag{2e}$$

where A_o is the outer tube cross-section area, A_c is the cross-section area of concrete, A_i is the inner tube cross-section area, A_{cn} is the nominal concrete area ($=\pi D_o^2/4$), f_{yo} is strength of outer tube ($=f_{0.2}$ for SS), f_{yi} is strength of inner tube, f_c' is unconfined concrete strength, ξ is confinement factor, χ is

void ratio (=D_i/D_o), and f_{scy} is nominal yield strength of composite sections. Due to the considerable strain hardening behaviour of SS material, the strength of the inner SS tube (f_{yi}) is approximately taken as the average value of yield strength ($f_{0.2}$) and ultimate strength (f_u). The strength of the inner FRP tube (f_{yi}) is taken as the averaged residual strength (σ_{res}) obtained from compression test on hollow section tubes.

The comparison between the test capacity (N_t) and predicted capacity (N_p) is summarized in Table 9, in which both the data in the present study and in [18] are included. The averaged value of N_p/N_t is 1.04 with coefficient of variance (COV) of 0.079, which suggests the design method in [18] can be adopted as a unified approach to predict the ultimate capacity of SWSSC-filled double-skin tubes with SS as the outer tube no matter what kind of inner tube (SS, GFRP, BFRP or CFRP) it is.

5.3 Fully SWSSC-filled CFRP and BFRP tubes

As the longitudinal strength of the FRP tube cannot be ignored, the current design method for concrete confined by FRP wraps, in which the longitudinal strength is ignored, is not suitable for fully concrete-filled FRP tubes. Based on the available data, Li et al. [18] proposed a new method to estimate the ultimate capacity of fully SWSSC-filled GFRP tubes. However, no design method has been reported for concrete-filled CFRP or BFRP tubes. Due to the limitation of available data, new method is not proposed in the present study. The method proposed by Li et al. [18] is adopted to estimate the ultimate capacity of fully SWSSC-filled CFRP and BFRP tubes. The formulae are listed below:

$$N_p = f_{un}(A_c + A_o \frac{f_{ul}}{f_{uh}}) \tag{3a}$$

$$\frac{f_{un}}{f_c'} = 1.12 + 2.64 \frac{f_l}{f_c'} \tag{3b}$$

$$f_l = \frac{2 f_{uh} t_o}{D_o} \tag{3c}$$

where N_p is predicted capacity, A_c is cross-section area of concrete, A_o is cross-section area of outer tube (i.e. FRP tube), f_{ul} is ultimate strength in longitudinal direction, f_{uh} is ultimate strength in hoop direction, f_c' is unconfined concrete strength, f_l is confining pressure, D_o is outer diameter of the outer tube, t_o is thickness of the outer tube, and f_{un} is nominal yielding strength. The relationship between f_{un}/f_c' and f_l/f_c' (i.e. Eq. (3b)) was determined by regression analysis as shown in Fig. 16, in which the dashed line represents Eq. (3b) and the data [16, 17, 18] for CFRP and BFRP tubes is also presented. As shown in Fig. 16, Eq. (3b) underestimates the confinement effect provided by CFRP tubes in a few cases.

A comparison between the test capacity and predicted capacity for fully SWSSC-filled FRP tubes is summarized in Table 10, in which the test data for GFRP is also included. Table 10 indicates that this method underestimates the capacity of fully SWSSC-filled CFRP tubes and the prediction for fully SWSSC-filled BFRP tubes is reasonable. This conservative prediction may be caused by the different material properties (e.g. f_{uh}) of CFRP and GFRP. Therefore, more study is needed on concrete-filled CFRP tubes to propose more appropriate design methods.

5.4 SWSSC-filled double-skin tubes (CFRP or BFRP as the outer tube)

Past research [16, 18] on concrete-filled double-skin tubes (GFRP as the outer tube) indicated that it is reasonable to assume that the ultimate capacity of the double-skin tubes is equal to the summation of the capacity of outer tube with sandwiched concrete, which behaves like fully concrete-filled tubes, and the capacity of inner tubes. The method proposed in [18] is adopted to estimate the ultimate capacity of double-skin tubes in the present study. They are summarised here for the convenience of readers.

$$N_p = N_{co} + N_i \tag{4a}$$

$$N_i = f_{yi} A_i \tag{4b}$$

where N_{co} is the capacity of the outer tube with sandwiched concrete, which can be determined by Eq. (3a), A_i is the cross-section area of the inner tube, and N_i is the capacity of the inner tube.

A comparison between the experimental capacity (N_t) and prediction (N_p) is summarized in Table 11, in which f_{yi} is strength of inner tube, f_{ul} is longitudinal strength of the outer tube, f_{uh} is hoop strength of the outer tube, f_c' is unconfined concrete strength, f_l is confining pressure, χ is void ratio (D_i/D_o). If the inner tube is SS, f_{yi} is the averaged value of yield strength ($f_{0.2}$) and ultimate strength (f_u). For the inner FRP tube, f_{yi} is taken as the averaged residual strength (σ_{res}).

As shown in Table 11, the prediction by the method in [18] is reasonable (Mean=0.94, COV=0.106), although the prediction for double-skin tubes with CFRP as the outer tube is slightly conservative.

As mentioned before some double-skin tubes (i.e. C165-C101-C, B114-B50-C, and B165-B101-C) did not fail by tube rupture. It should pointed out that the method adopted herein is based on the assumption that the outer FRP tube can reach the hoop strength (f_{uh}). Although the prediction is quite close the experimental data, more studies are needed to investigate the hoop stress in the outer tube for concrete-filled double skin tubes with FRP as both the outer and inner tubes.

6. Conclusions

This paper presents an experimental investigation on SWSSC-filled SS, CFRP and BFRP tubular stub columns under axial compression. Both the fully SWSSC-filled tubes and SWSSC-filled double-skin tubes with different combinations of tube materials were tested. Several conclusions can be made as follows:

(1) The strength and ductility of SWSSC-filled tubes are significantly enhanced in comparison with hollow section tubes and plain concrete.

(2) Among the three FRPs investigated, CFRP has the highest ultimate strength and elastic moduli in both longitudinal and transverse directions. BFRP has the lowest ultimate strength and elastic modulus in longitudinal direction, while the material properties of BFRP in hoop direction are similar to those of GFRP. The ultimate strain of CFRP is much less than that of BFRP and GFRP.

(3) The confinement effect provided by SS tubes is lower than that by CFRP and BFRP tubes, but the confinement can be maintained for larger axial strain for SS tubes. The strength enhancement and ductility of SWSSC-filled CFRP tubes are higher than those of BFRP tubes mainly due to its higher hoop strength. The confinement provided by BFRP and GFRP tubes is quite similar.

(4) For some of the double-skin tubes with FRP as both the outer and inner tubes, the outer tube rupture did not occur as the inner FRP cannot effectively restrain the lateral expansion of concrete after the axial strain reaches around 0.03.

(5) As the diameter-to-thickness ratio of tubes increases, the level of confinement reduces for all the four types of tubes (SS, GFRP, BFRP and CFRP). When compared with fully filled tubes, the confinement provided by the double skin tubes start to decrease at large deformation due to the buckling of inner FRP tubes. The influence of inner tube on confinement is not significant unless they are slender FRP tubes after an axial strain of 0.03.

(6) The formulae proposed in [18] can be adopted as a unified approach to estimate the ultimate capacity of SWSSC-filled SS, GFRP, CFRP and BFRP tubes. In general, the prediction is in reasonable agreement to the test data although the capacity estimation of SWSSC-filled CFRP tubes is slightly conservative.

Research is being conducted on the long-term behavior of SWSSC and the shrinkage effect on the confinement. The existing work in the literature [28-31] on the behaviour of normal composite concrete-filled steel tubular columns under chloride corrosion will be consulted.

Acknowledgement

The authors wish to acknowledge the financial support provided by the Australian Research Council (ARC) through an ARC Discovery Grant (DP160100739), and CST composites for suppling the GFRP tubes. The tests were conducted in the Civil Engineering Laboratory at Monash University. Thanks are also due to Mr. Long Goh, Mr. Saravanan Mani and Mr. Jeff Doddrell for

their assistance. We thank Mr. Damian Carr of Bayside City Council for his permission to obtain seawater and sea sand from Brighton Beach in Melbourne.

References

[1] X.L. Zhao, L.H. Han, H. Lu, Concrete-filled tubular members and connections, Taylor & Francis, Oxford, UK, 2010.

[2] X.L. Zhao, L.H. Han, Double skin composite construction, Progress in Structural Engineering and Materials, 8(3) (2006) 93-102.

[3] J.G. Teng, T. Yu, Y.L. Wong, S.L. Dong, Hybrid FRP–concrete–steel tubular columns: Concept and behaviour, Construction and Building Materials, 21(4) (2007) 846-854.

[4] S.K. Kaushik, S. Islam, Suitability of sea water for mixing structural concrete exposed to a marine environment, Cement and Concrete Composites, 17(3) (1995) 177-185.

[5] K. Kupwade-Patil, E. Allouche, Impact of alkali silica reaction on fly ash-based Geopolymer concrete, Journal of Materials in Civil Engineering, ASCE, 25(1) (2013) 131-139.

[6] T.U.T. Mohammed, H. Hamada, T. Yamaji, Performance of seawater-mixed concrete in the tidal environment, Cement and Concrete Research, 34(4) (2004) 593-601.

[7] D. Lam, L. Gardner, Structural design of stainless steel concrete filled columns, Journal of Constructional Steel Research, 64(11) (2008) 1275-1282.

[8] B. Uy, Z. Tao, L.H. Han, Behaviour of short and slender concrete-filled stainless steel tubular columns, Journal of Constructional Steel Research, 67(3) (2011) 360-378.

[9] V. Lopresto, C. Leone, I. de Iorio, Mechanical characterisation of basalt fibre reinforced plastic, Composites: Part B, 42(2011) 717-723.

[10] ACI 440.2R-08. Guide for the Design and Construction of Externally Bonded FRP Systems for Strengthening Concrete Structures, American Concrete Institute, Farmington Hills, MI, 2008.

[11] J.G. Teng, L. Lam, Behavior and modelling of fiber reinforced polymer-confined concrete, Journal of Structural Engineering, 130(2004) 1713-1723.

[12] J.G. Teng, T. Jiang, L. Lam, Y.Z. Luo, Refinement of a design-oriented stress–strain model for frp-confined concrete, Journal of Composites for Construction, 13(4) (2009) 269-278.

[13] T. Ozbakkaloglu, J.C. Lim, T. Vincent, FRP-confined concrete in circular sections: Review and assessment of stress–strain models, Engineering Structures, 49(2013) 1068-1088.

[14] J.G. Teng, T. Yu, J.G. Dai, G.M. Chen, FRP composites in new construction: current status and opportunities, in: Proceedings of 7th National Conference on FRP Composites in Infrastructure (Supplementary Issue of Industrial Construction), keynote presentation, 2011.

[15] J.G. Teng, Performance enhancement of structures through the use of fibre-reinforced polymer (FRP) composites, in: Proceedings of 23rd Australasian Conference on the Mechanics of Structures and Materials (ACMSM23), Lismore, Australia, keynote presentation, 2014.

[16] A.Z. Fam, S.H. Rizkalla, Behavior of axially loaded concrete - filled circular fiber - reinforced polymer tubes, ACI Structural Journal, 98(3) (2001) 280-289.

[17] B. Zhang, T. Yu, J.G. Teng, Behavior of concrete-filled FRP tubes under cyclic axial compression, Journal of composites for construction, 3(19) (2015) 04014060.

[18] Y.L. Li, X.L. Zhao, R.K. Raman Singh, S. Al-Saadi, Experimental study on seawater and sea sand concrete filled GFRP and stainless steel tubular stub columns, Thin-Walled Structures 106(2016) 390-406.

[19] AS/NZS 4673:2001. Cold-formed stainless steel structures, Standards Australia, Sydney, 2001.

[20] AS 1391-2007. Metallic materials-Tensile testing at ambient temperature, Standards Australia, Sydney, 2007.

[21] ASTM D3039/D3039M-14. Standard test method for tensile properties of polymer matrix composite materials, American Society for Testing and Materials, West Conshohocken, PA, 2014.

[22] ASTM D2290-12. Standard test method for apparent hoop tensile strength of plastic or reinforced plastic pipe, American Society for Testing and Materials, West Conshohocken, PA, 2012.

[23] Z.F. Chen, L.L. Wan, S. Lee, M. Ng, J.M. Tang, M. Liu, L. Lee, Evaluation of CFRP, GFRP and BFRP material systems for the strengthening of RC Slabs, Journal of Reinforced Plastics and Composites, 27(12) (2008) 1233-1243.

[24] T. Ozbakkaloglu, T. Xie, Geopolymer concrete-filled FRP tubes: Behavior of circular and square columns under axial compression, Composites Part B, 96(2016) 215-230.

[25] L.H. Han, G.H. Yao, X.L. Zhao, Tests and calculations for hollow structural steel (HSS) stub columns filled with self-consolidating concrete (SCC), Journal of Constructional steel research, 61(2005) 1241-1269.

[26] V.W.Y. Tam, Z.B. Wang, Z. Tao, Behaviour of recycled aggregate concrete filled stainless steel stub columns, Materials and Structures, 47(2014) 293-310.

[27] Y.F. Yang, G.L. Ma, Experimental behaviour of recycled aggregate concrete filled stainless steel tube stub columns and beams, Thin-walled Structures, 66(2013) 62-75.

[28] L.H. Han, C.C. Hou, Q.L. Wang, Behavior of circular CFST stub columns under sustained load and chloridecorrosion, Journal of Constructional Steel Research, 103(2014) 23-36.

[29] L.H. Han, C. Hou, Q.L. Wang, Square concrete filled steel tubular (CFST) members under loading and chloride corrosion: Experiments, Journal of Constructional Steel Research, 71(2012) 11-25.

[30] C. Hou, L.H. Han, X.L. Zhao, Full-range analysis on square CFST stub columns and beams under loading and chloride corrosion, Thin-Walled Structures, 68(2013) 50-64.

[31] W. Li, L.H. Han, X.L. Zhao, Behavior of CFDST stub columns under preload, sustained load and chloride corrosion, Journal of Constructional Steel Research, 107(2015) 12-23.

Figures

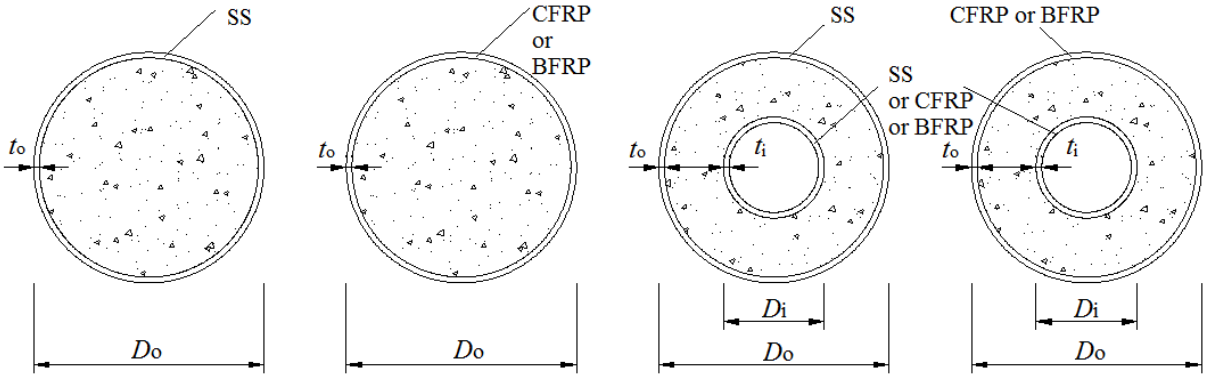

(a) Fully SWSSC-filled tubes (b) SWSSC-filled double-skin tubes

Fig. 1. Illustration of cross-sections (a) fully SWSSC-filled tubes (b) SWSSC-filled double-skin tubes.

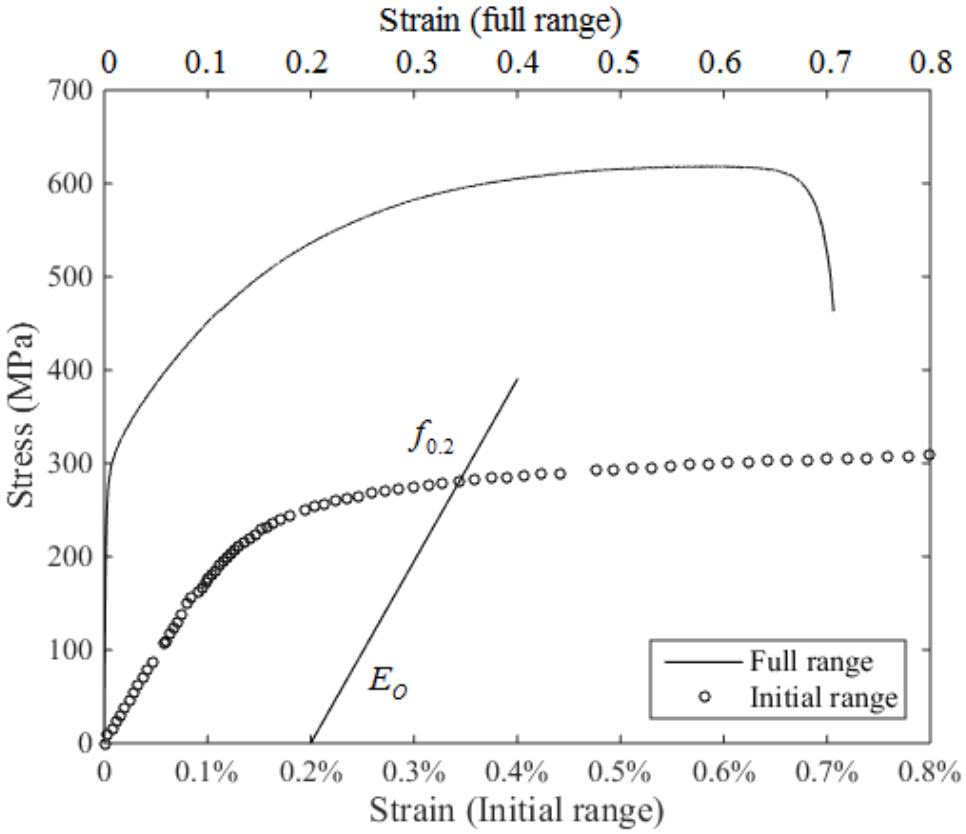

Fig. 2. Typical stress-strain curve of stainless steel.

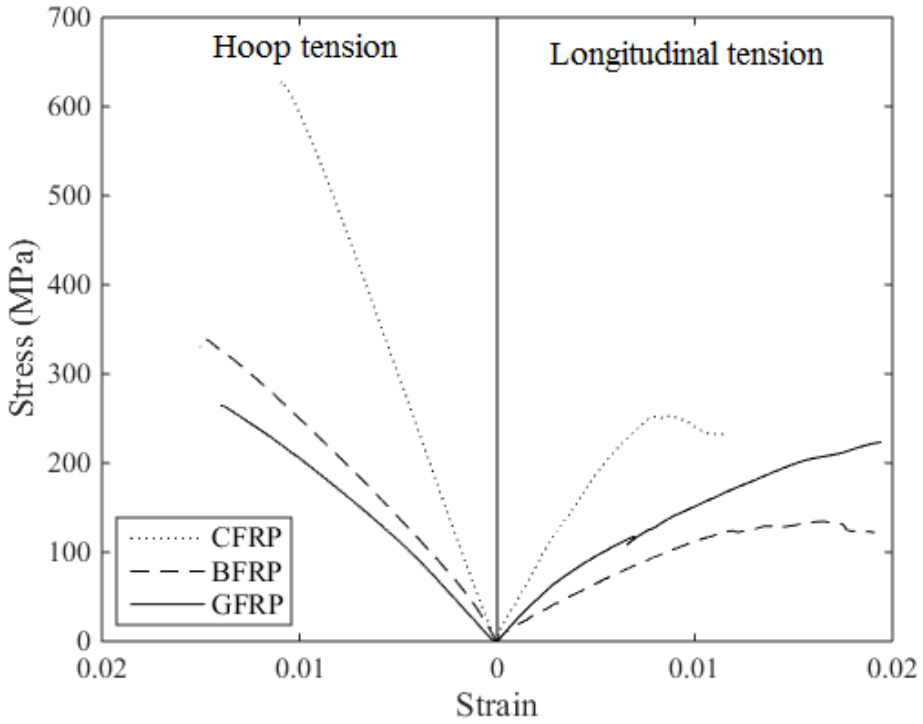

Fig. 3. Typical stress-strain curves of CFRP, BFRP and GFRP (the data of GFRP is from Li et al. 2016).

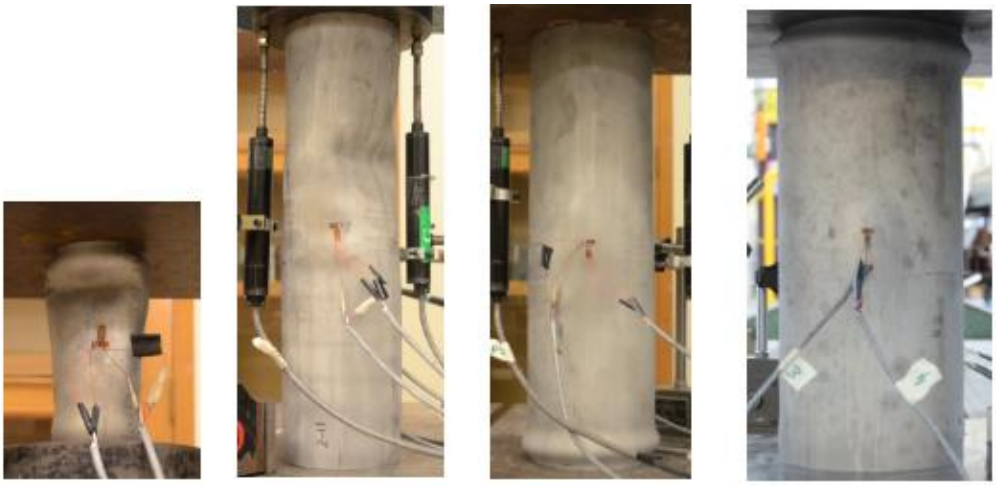

Fig. 4. Failure modes of SS hollow sections.

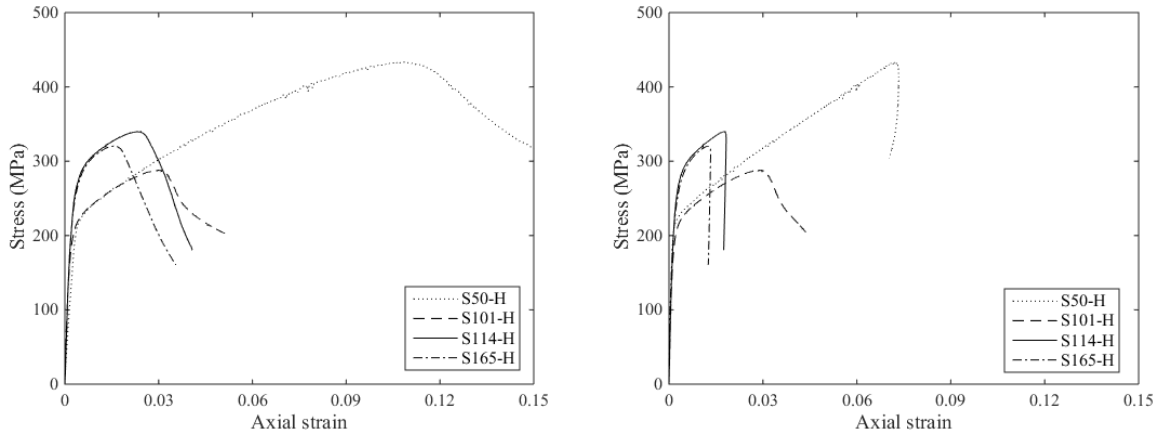

(a) Axial strain obtained from LVDTs (b) Axial strain obtained from strain gauges

Fig. 5. Stress-strain curves of SS hollow sections (a) axial strain obtained from LVDTs (b) axial strain obtained from strain gauges.

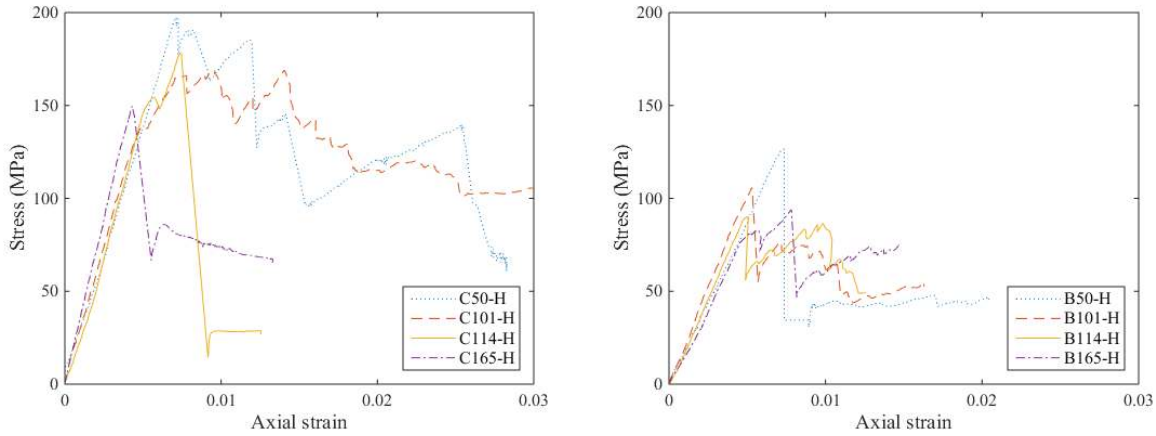

(a) Axial strain obtained from LVDT

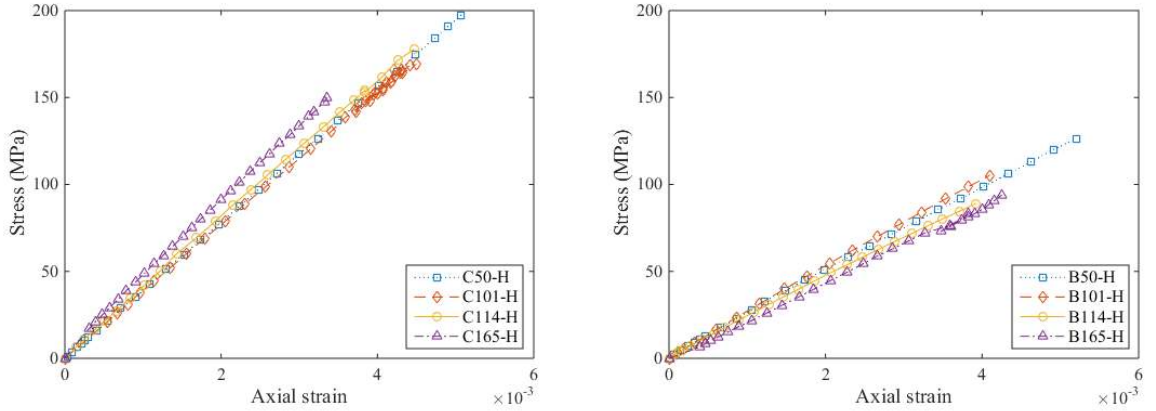

(b) Axial strain obtained from strain gauge

Fig. 6. Stress-strain curves of CFRP and BFRP hollow section (a) axial strain obtained from LVDT (b) axial strain obtained from strain gauge.

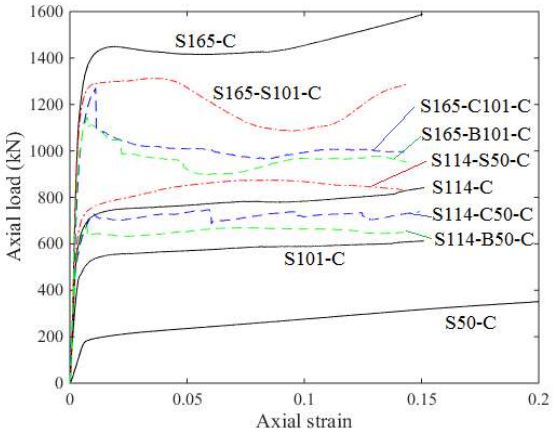

(a) SWSSC-filled SS tubes

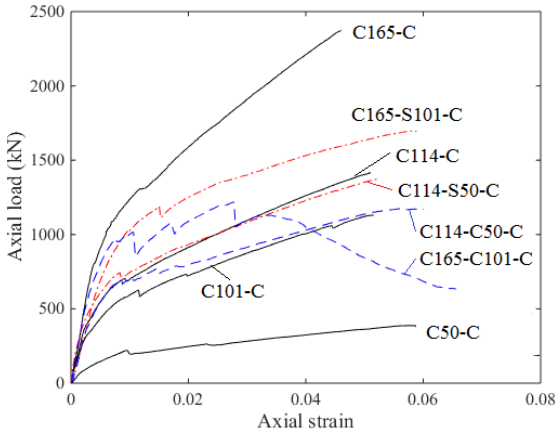

(b) SWSSC-filled CFRP tubes

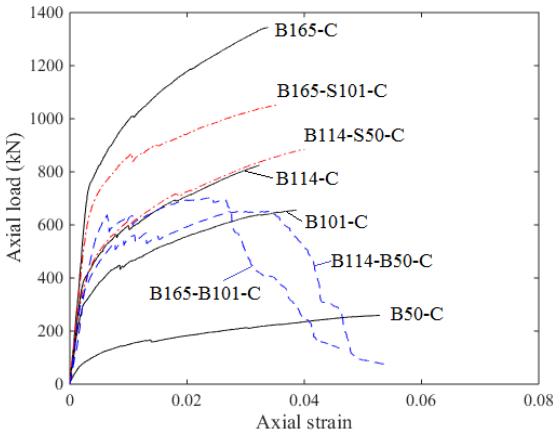

(c) SWSSC-filled BFRP tubes.

Fig. 7. Load-axial strain curves of SWSSC-filled tubes (a) SWSSC-filled SS tubes (b) SWSSC-filled CFRP tubes (c) SWSSC-filled BFRP tubes.

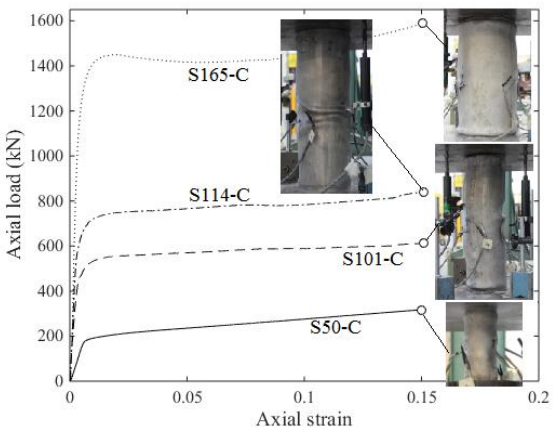

(a) Fully filled SS tubes

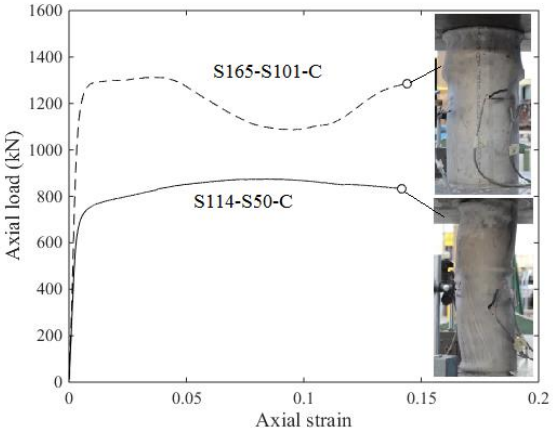

(b) Double-skin tubes (SS as both outer and inner tubes)

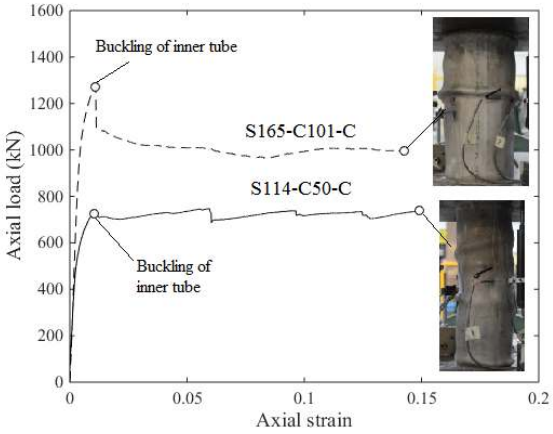

(i)

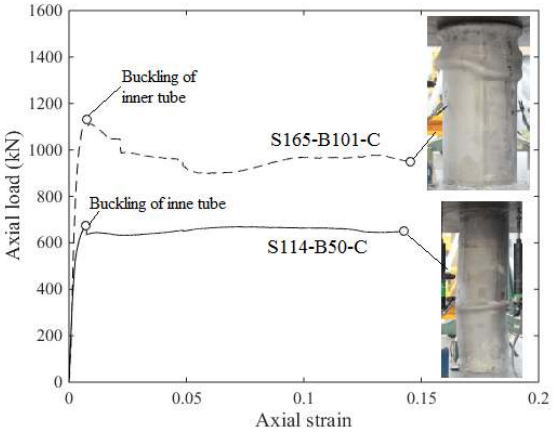

(ii)

(c) double-skin tubes (SS as the outer tube and CFRP/BFRP as the inner tube)

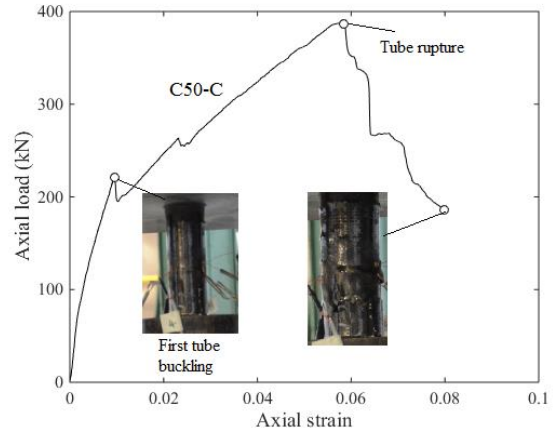

(i)

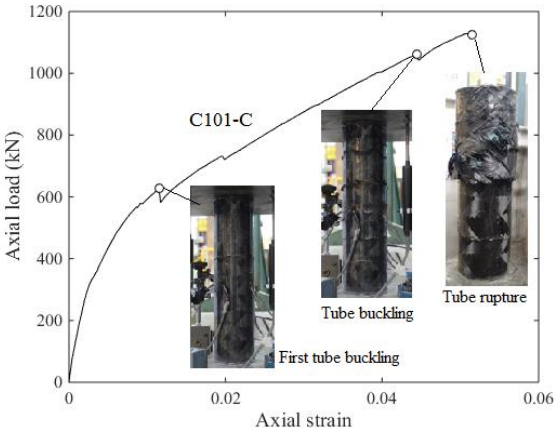

(ii)

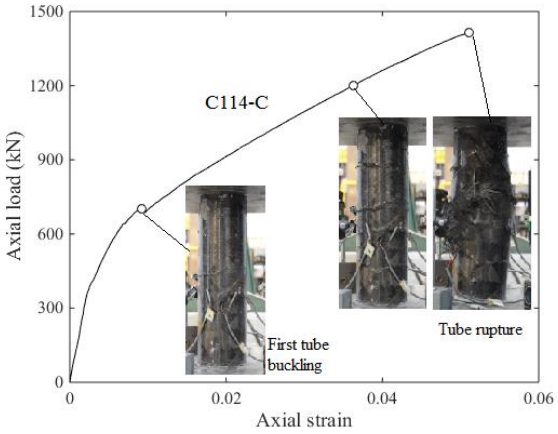

(iii)

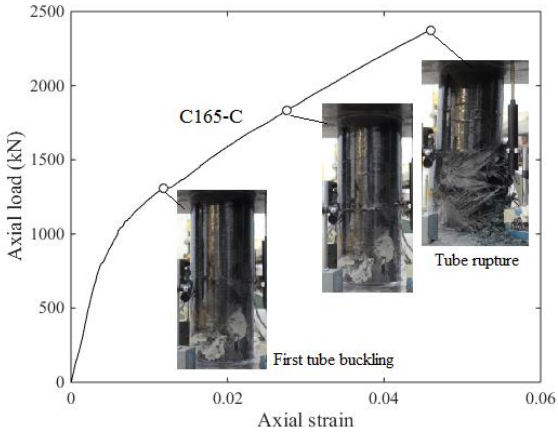

(iv)

(d) fully filled CFRP tubes

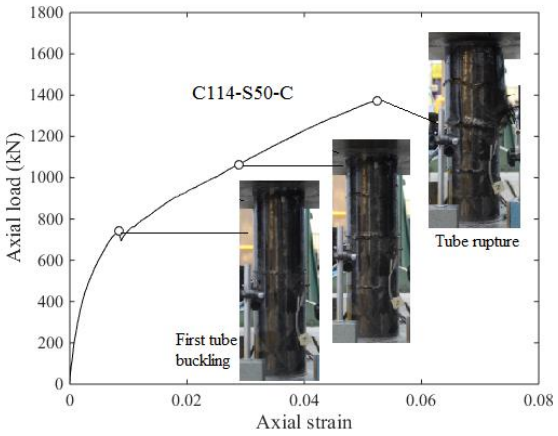

(i)

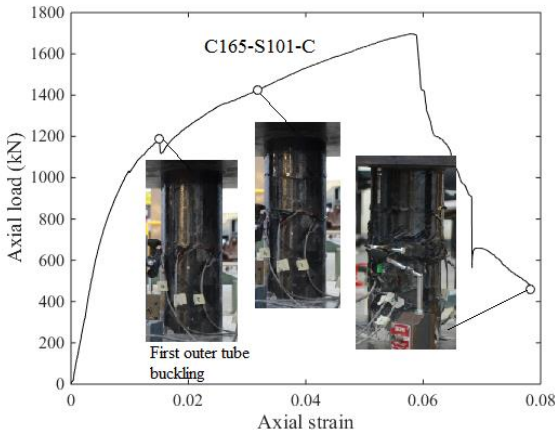

(ii)

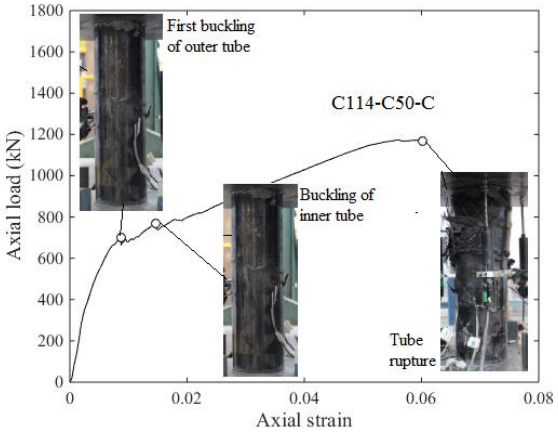

(iii)

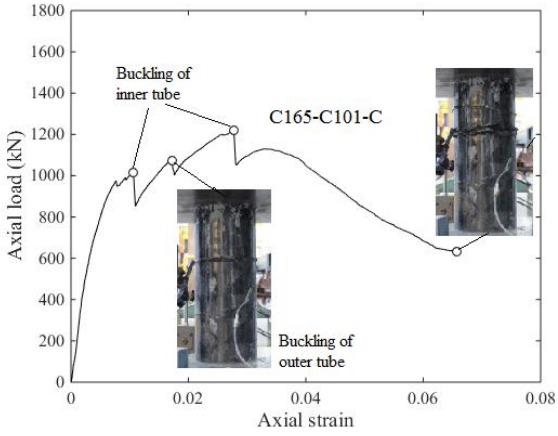

(iv)

(e) double-skin tubes (CFRP as the outer tube)

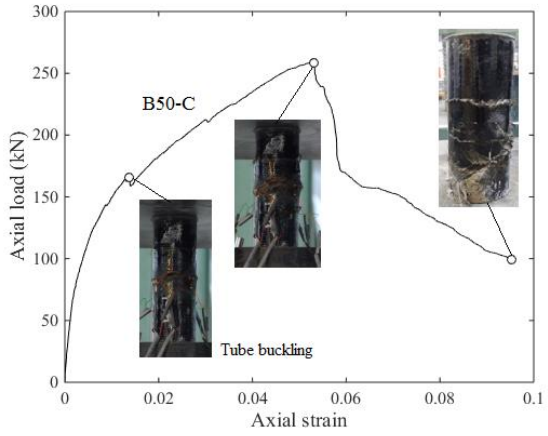

(i)

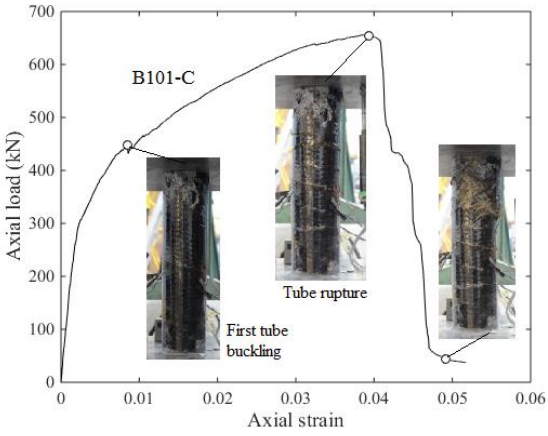

(ii)

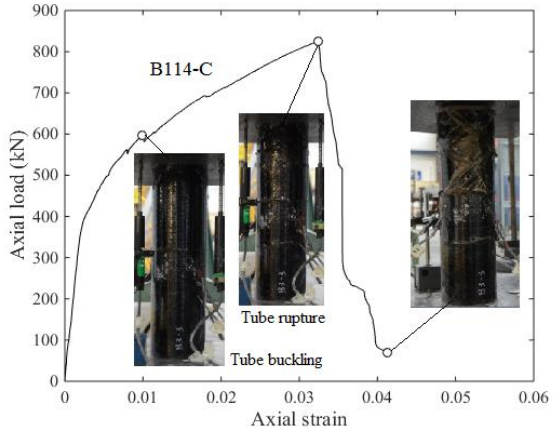

(iii)

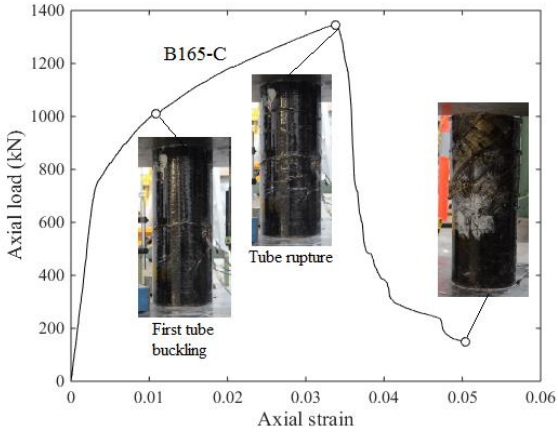

(iv)

(f) fully filled BFRP tubes

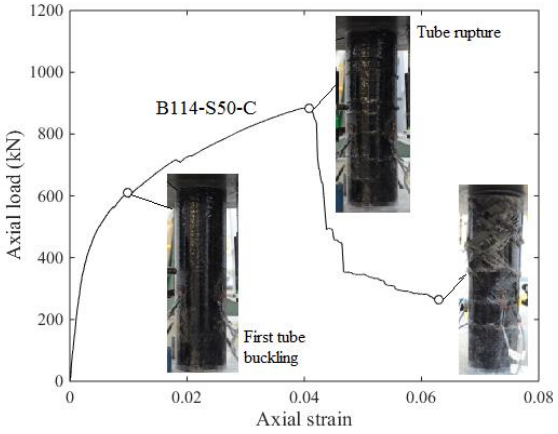

(i)

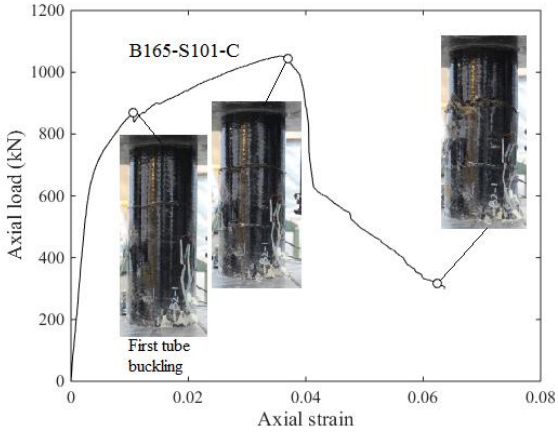

(ii)

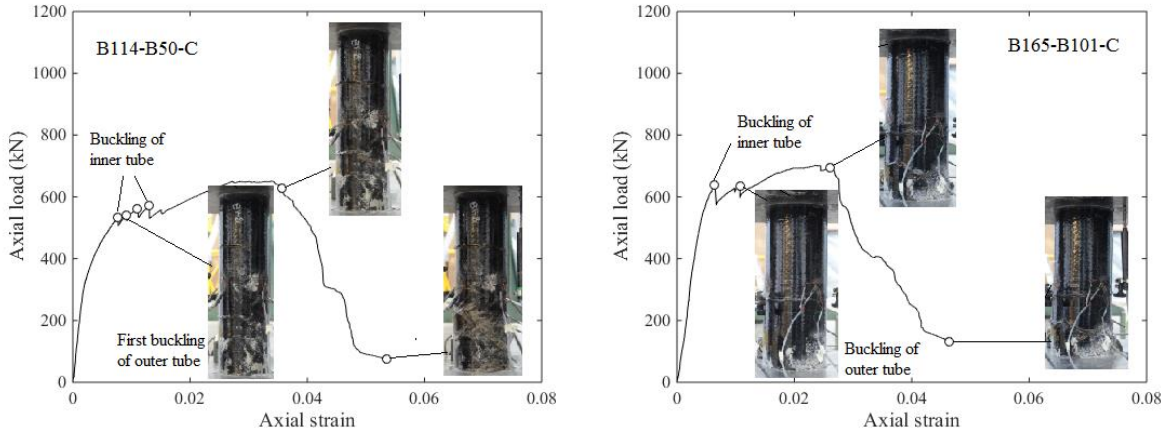

(iii) (iv)

(g) double-skin tubes (BFRP as the outer tube)

Fig. 8. Load-axial strain curves and failure modes (a) fully filled SS tubes (b) double-skin tubes (SS as both outer and inner tubes) (c) double-skin tubes (SS as the outer tube and CFRP/BFRP as the inner tube) (d) fully filled CFRP tubes (e) double-skin tubes (CFRP as the outer tube) (f) fully filled BFRP tubes (g) double-skin tubes (BFRP as the outer tube).

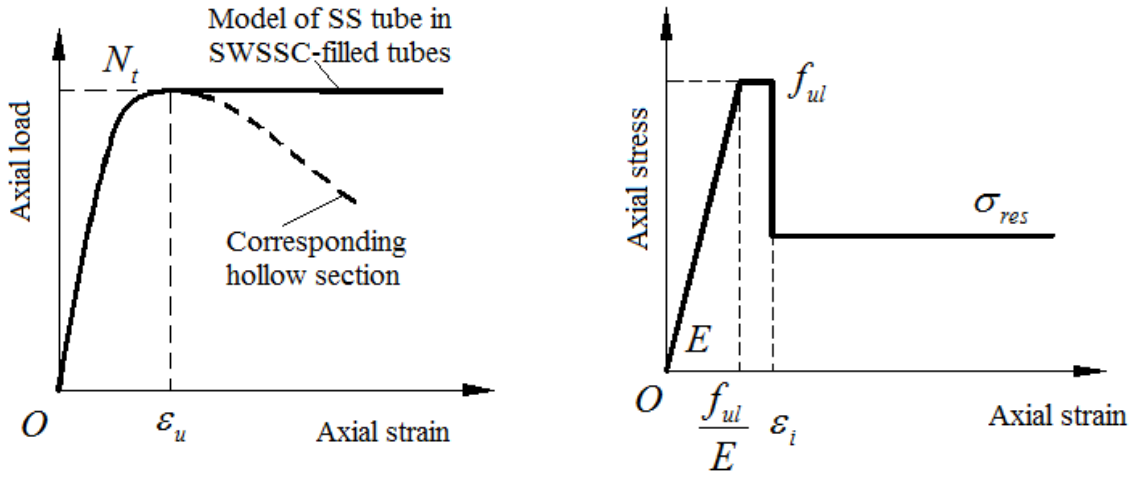

(a) Stainless steel tube (b) CFRP and BFRP inner tube

Fig. 9. Simplified stress-strain models (a) stainless steel tube (b) CFRP and BFRP inner tube.

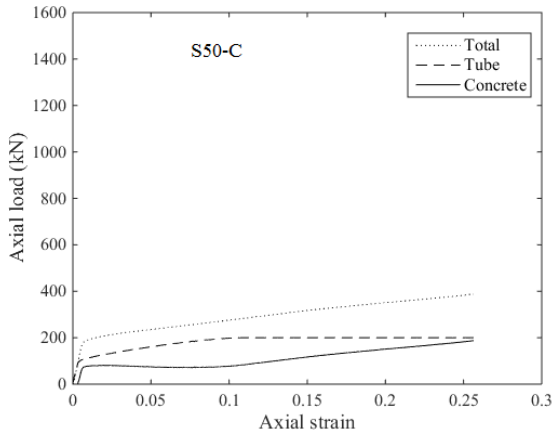

(i)

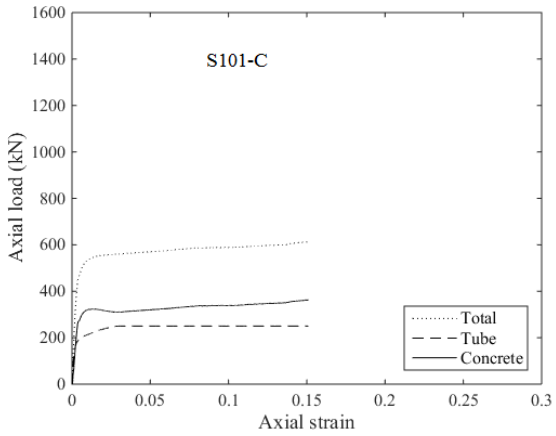

(ii)

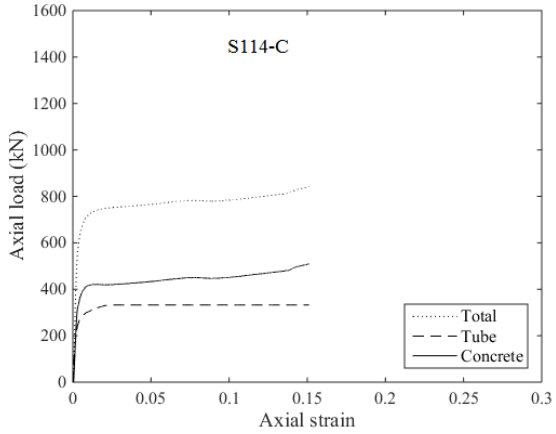

(iii)

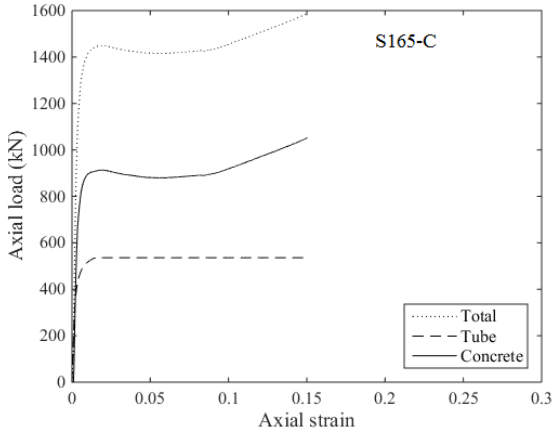

(iv)

(a) Fully filled SS tubes

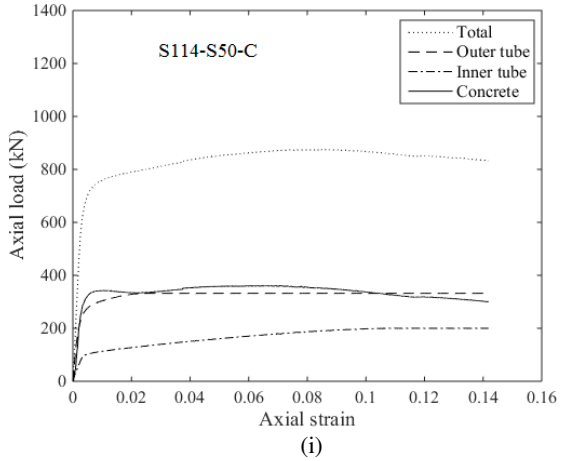

(i)

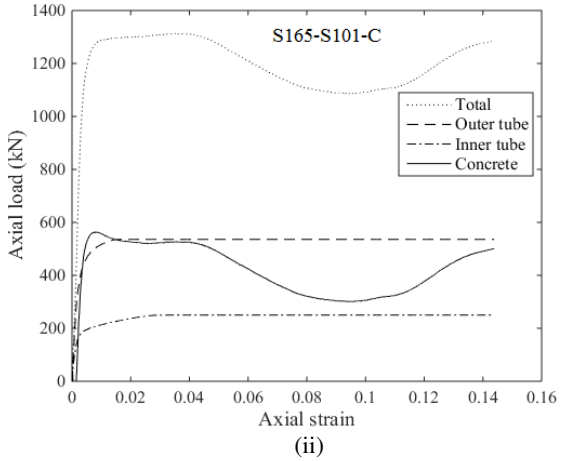

(ii)

(b) Double-skin tubes (SS as both outer and inner tubes)

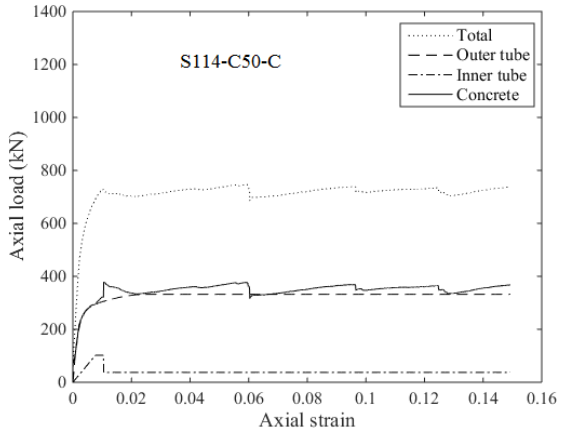

(i)

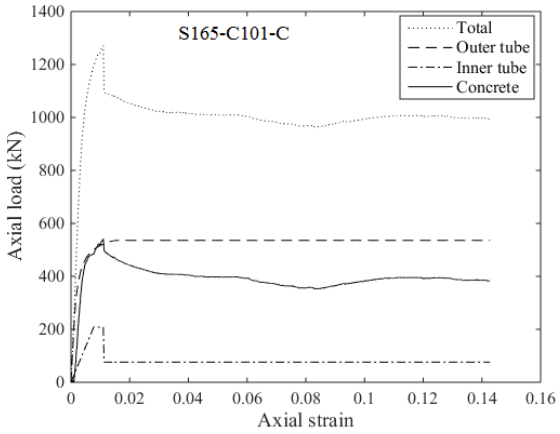

(ii)

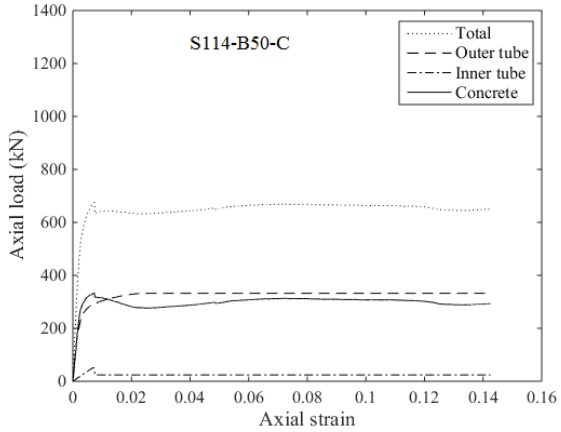

(iii)

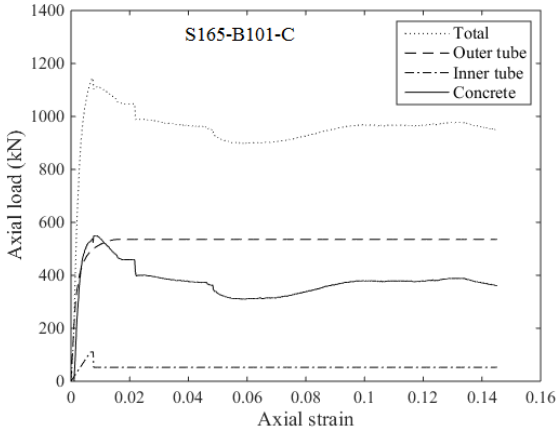

(iv)

(c) Double-skin tubes (SS as the outer tube and CFRP/BFRP as the inner tube)

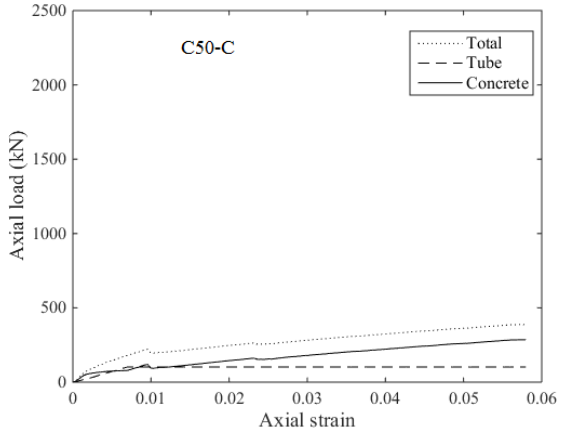

(i)

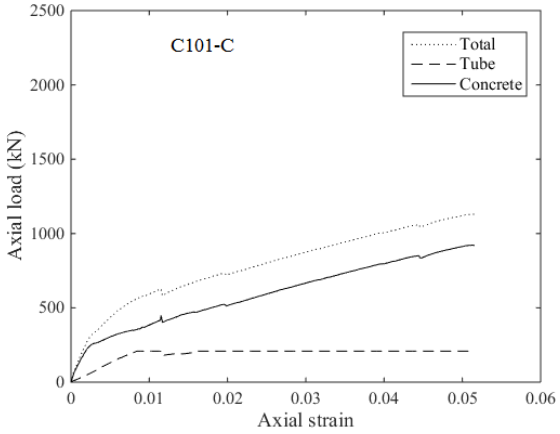

(ii)

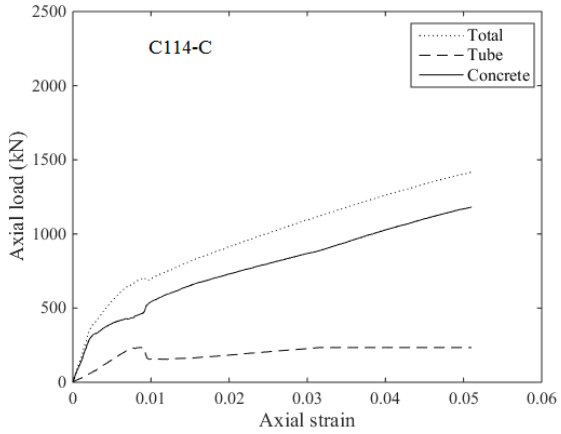

(iii)

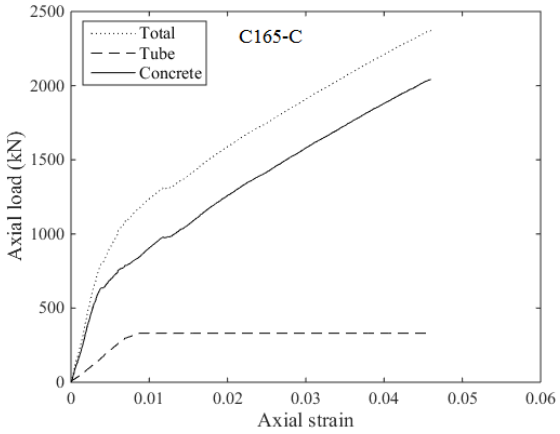

(iv)

(d) Fully filled CFRP tubes

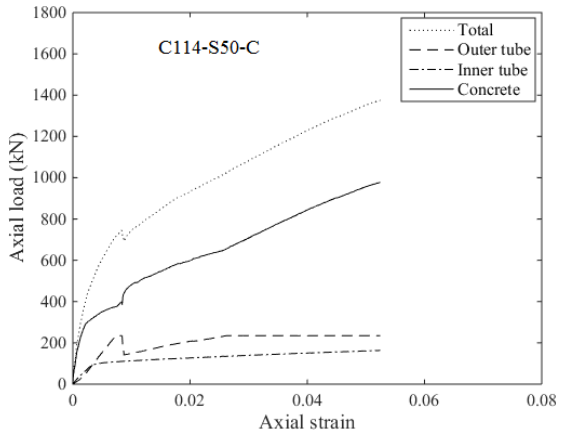

(i)

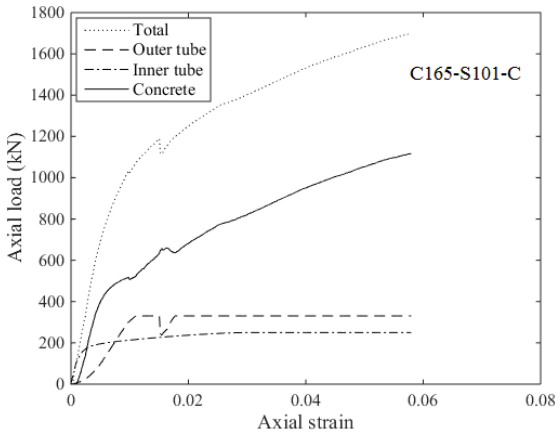

(ii)

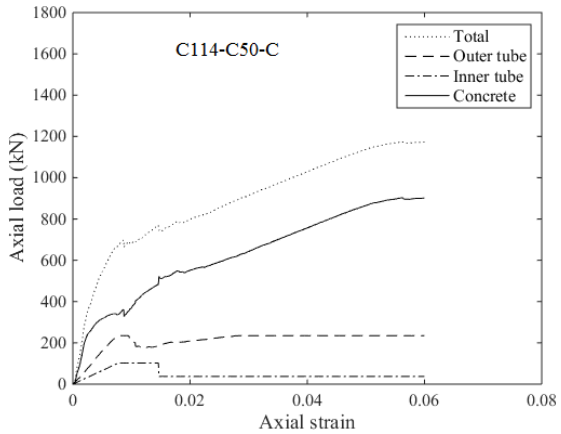

(iii)

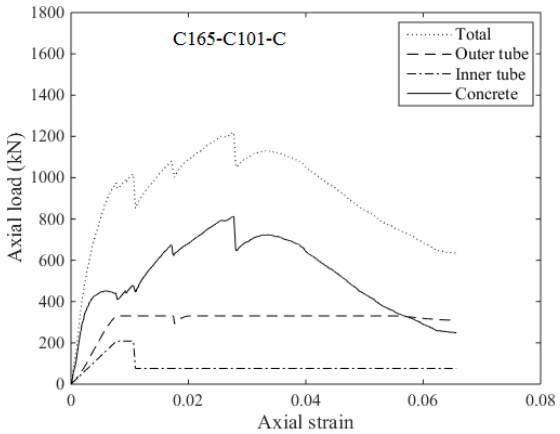

(iv)

(e) Double-skin tubes (CFRP as the outer tube)

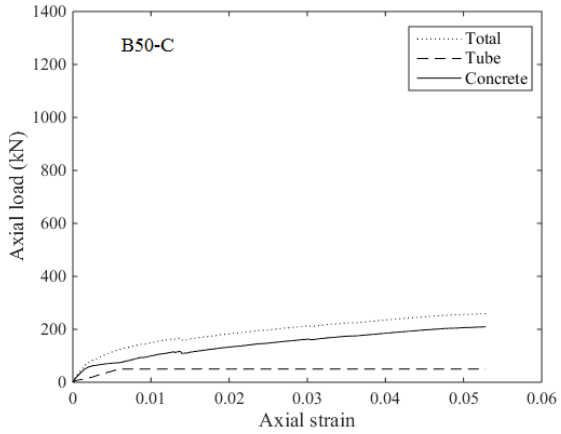

(i)

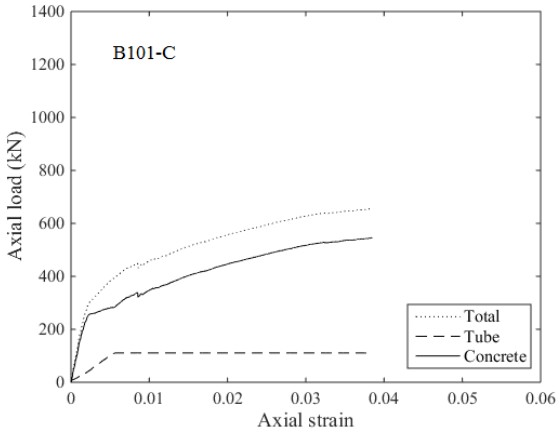

(ii)

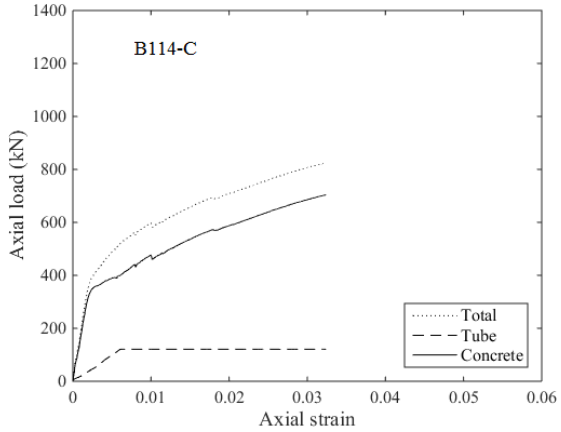

(iii)

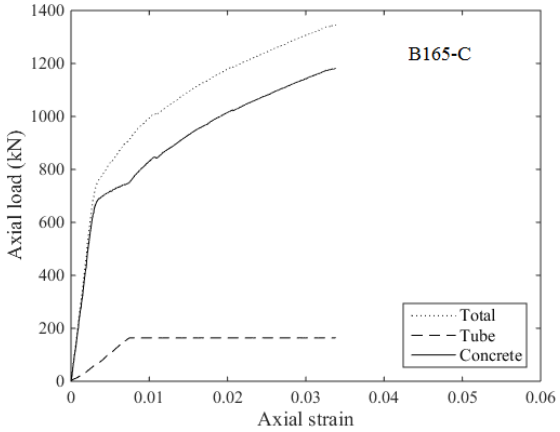

(iv)

(f) Fully filled BFRP tubes

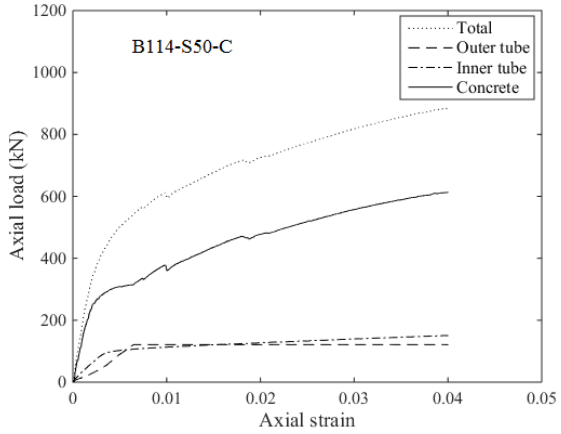

(i)

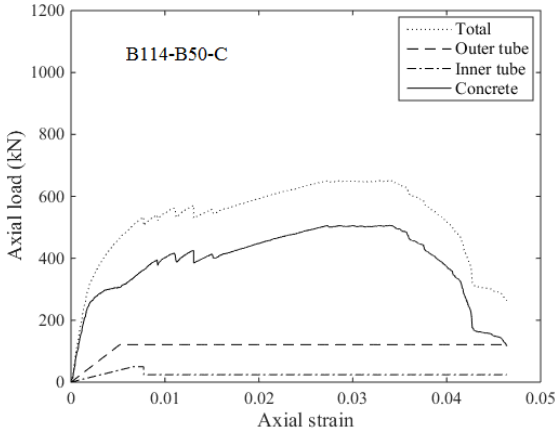

(ii)

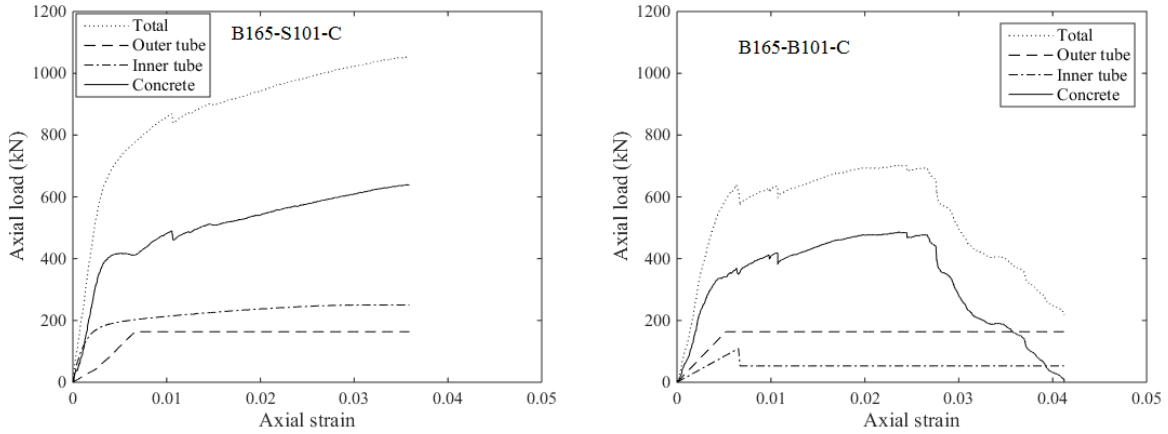

(g) double-skin tubes (BFRP as the outer tube).

Fig. 10. Load distribution: (a) fully filled SS tubes (b) double-skin tubes (SS as both outer and inner tubes) (c) double-skin tubes (SS as the outer tube and CFRP/BFRP as the inner tube) (d) fully filled CFRP tubes (e) double-skin tubes (CFRP as the outer tube) (f) fully filled BFRP tubes (g) double-skin tubes (BFRP as the outer tube).

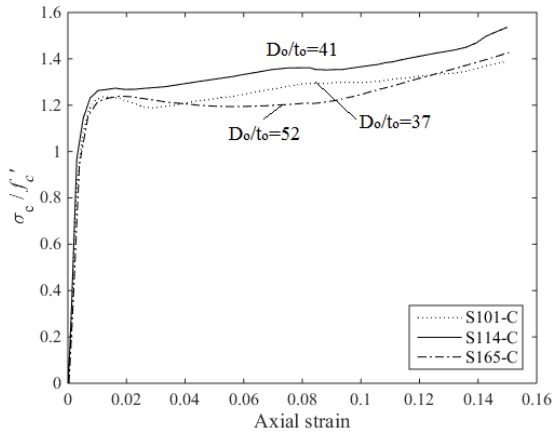

(a) Fully SWSSC-filled SS tubes

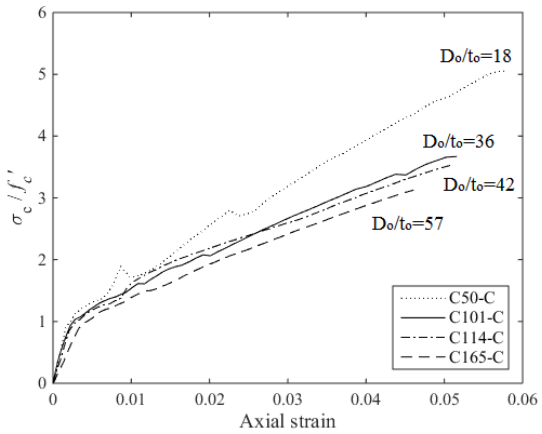

(b) Fully SWSSC-filled CFRP tubes

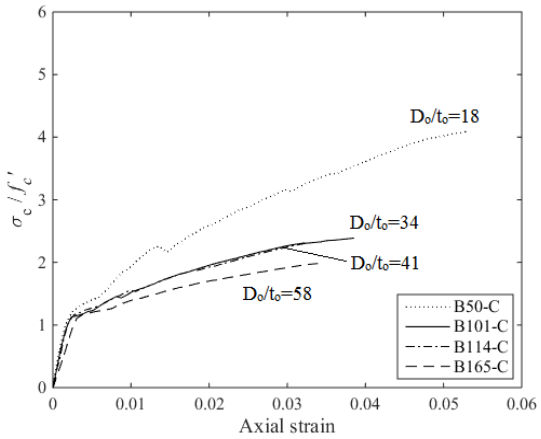

(c) Fully SWSSC-filled BFRP tubes

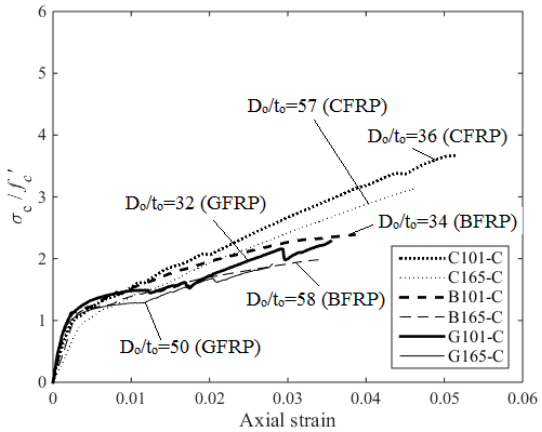

(d) Fully SWSSC-filled FRP tubes

Fig. 11. Effects of tube diameter-to-thickness ratio (a) fully SWSSC-filled SS tubes (b) fully SWSSC-filled CFRP tubes (c) fully SWSSC-filled BFRP tubes (d) Fully SWSSC-filled FRP tubes.

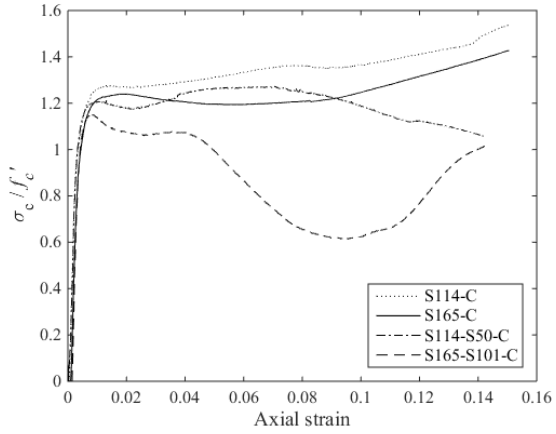

(i)

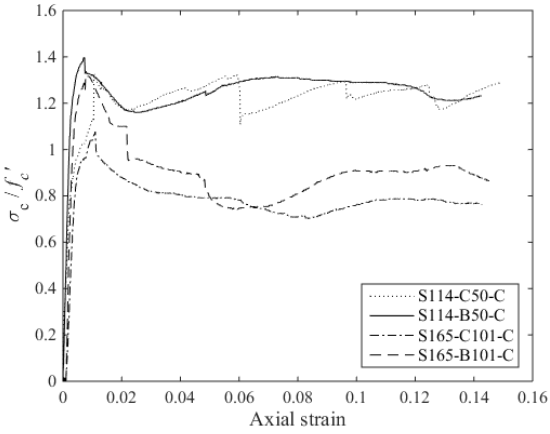

(ii)

(a) SWSSC-filled SS tubes

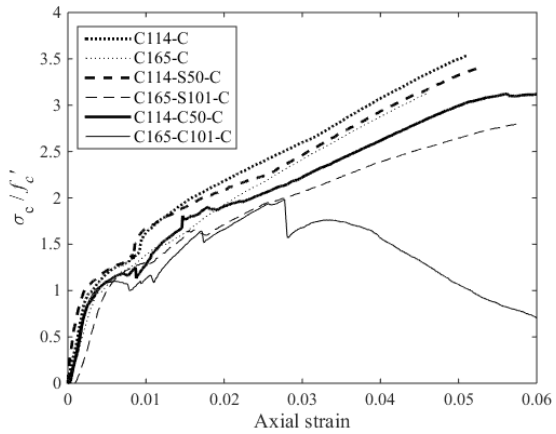

(b) SWSSC-filled CFRP tubes

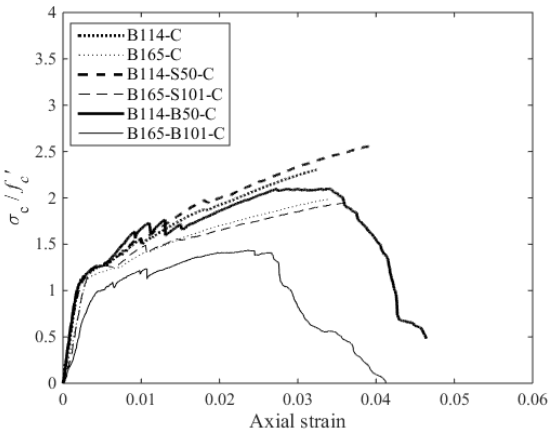

(c) SWSSC-filled BFRP tubes

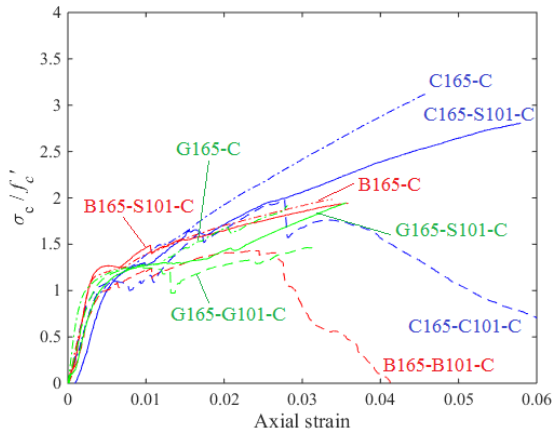

(d) SWSSC-filled FRP tubes

Fig. 12. Effects of cross-section types (a) SWSSC-filled SS tubes (b) SWSSC-filled CFRP tubes (c) SWSSC-filled BFRP tubes (d) SWSSC-filled FRP tubes.

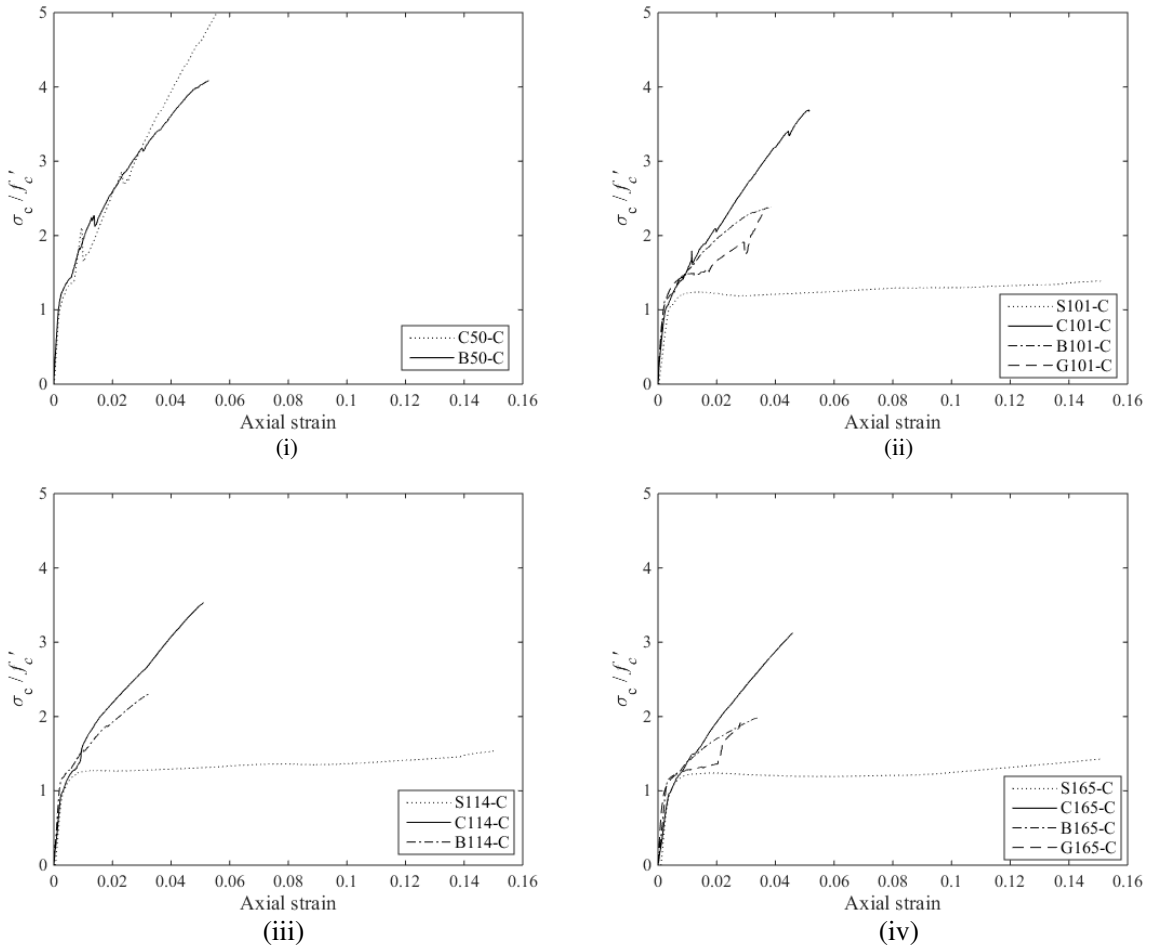

(i) (ii) (iii) (iv)

(a) Fully filled tubes

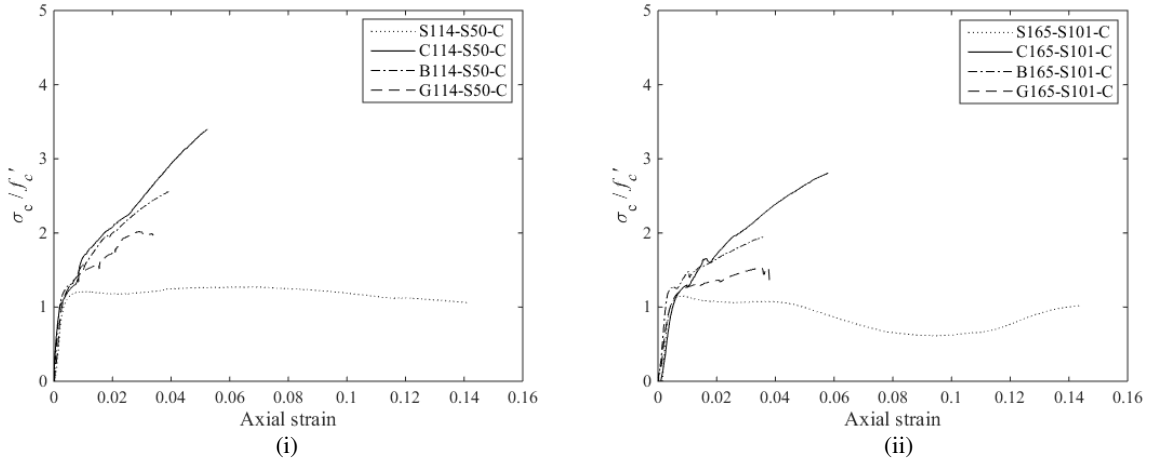

(i) (ii)

(b) Double-skin tubes

Fig. 13. Effects of outer tube type (a) Fully filled tubes (b) Double-skin tubes.

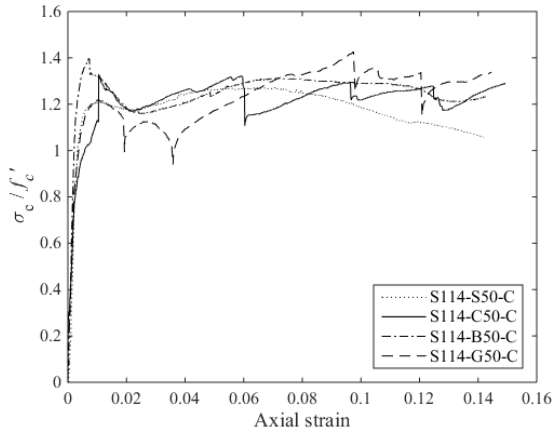

(i)

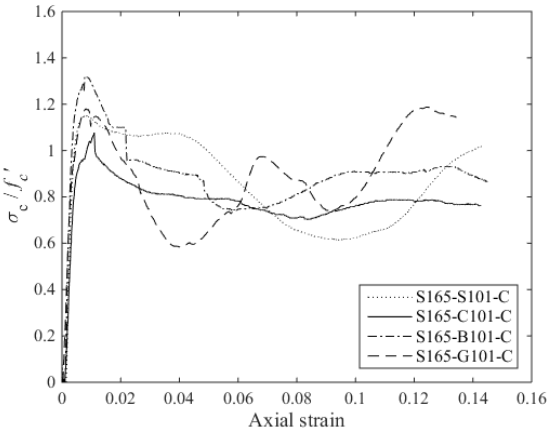

(ii)

(a) double-skin tubes (SS as the outer tube)

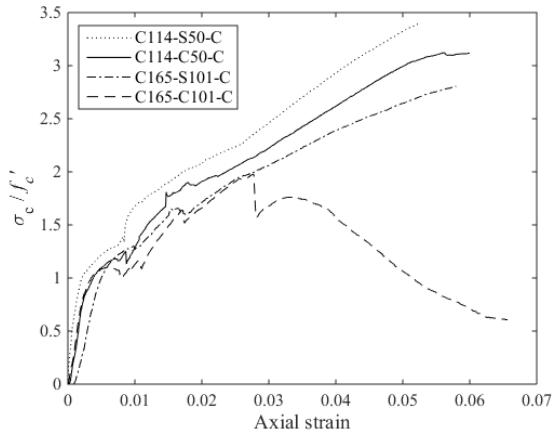

(b) double-skin tubes (CFRP as the outer tube)

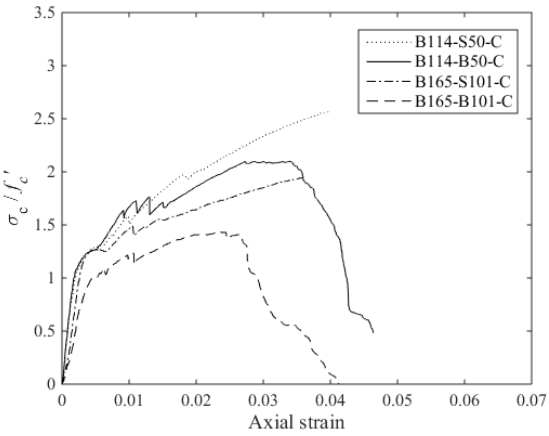

(c) double-skin tubes (BFRP as the outer tube)

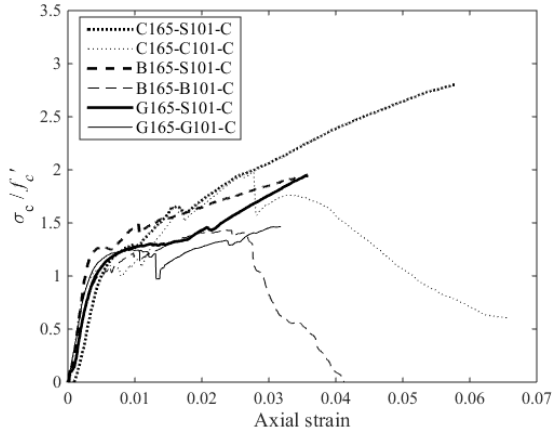

(d) double-skin tubes (FRP as the outer tube)

Fig. 14. Effects of inner tube type (a) double-skin tubes (SS as the outer tube) (b) double-skin tubes (CFRP as the outer tube) (c) double-skin tubes (BFRP as the outer tube) (d) double-skin tubes (FRP as the outer tube).

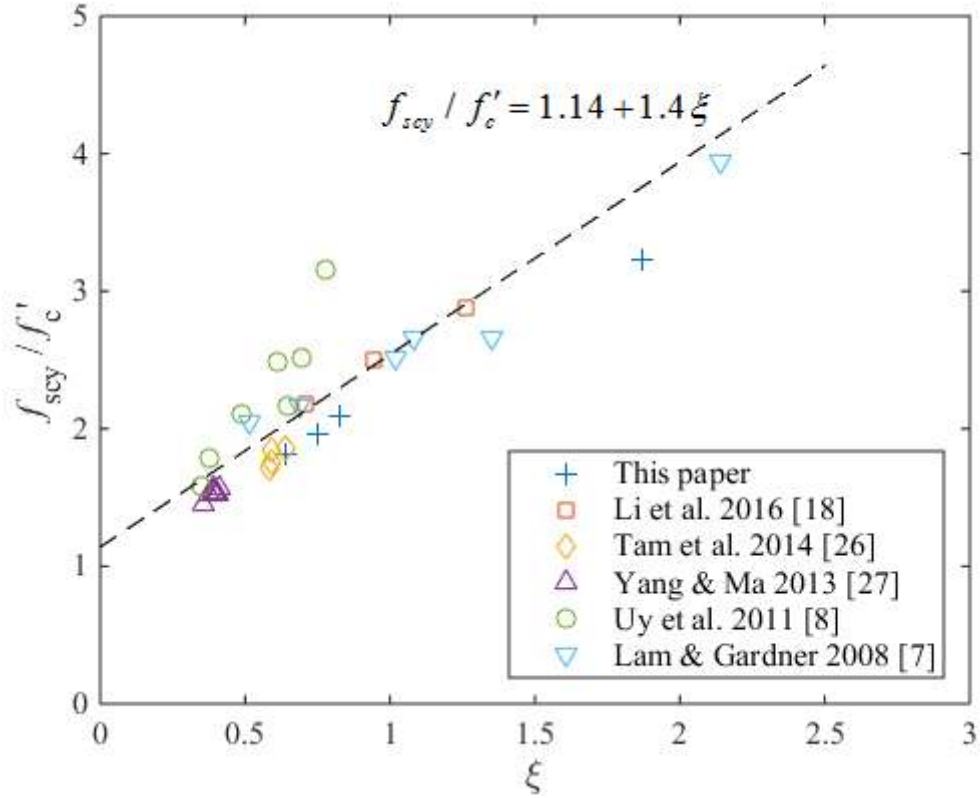

Fig. 15. Regression analysis of existing data for concrete-filled SS tubes.

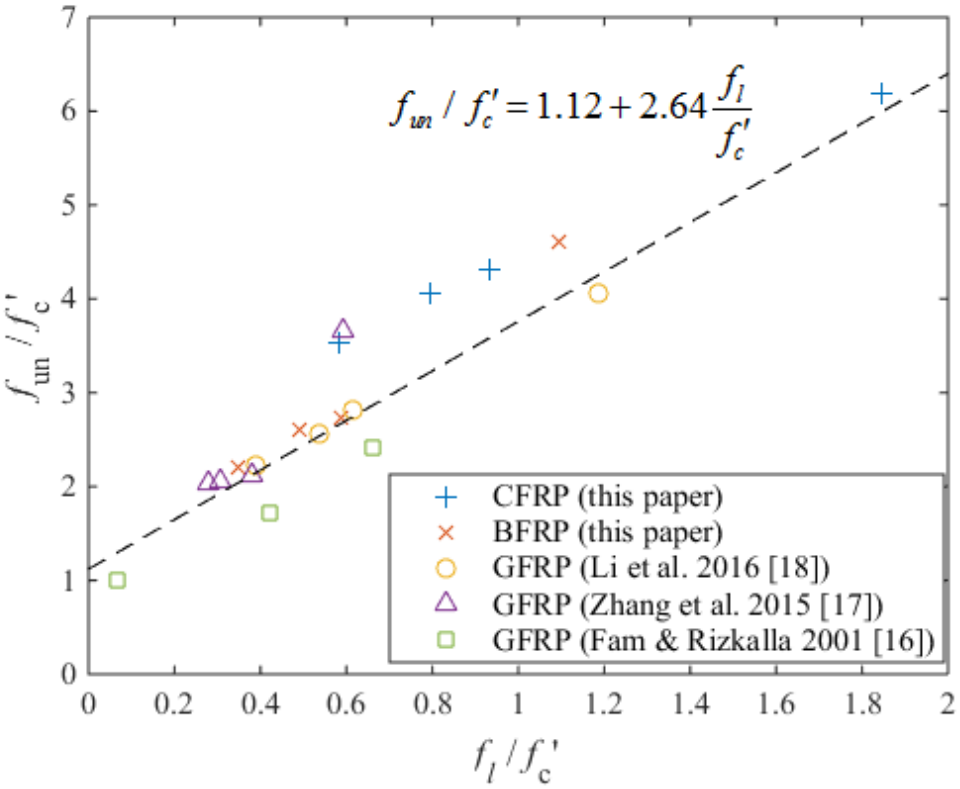

Fig. 16. Regression analysis of existing data for concrete-filled FRP tubes.

Tables

Table 1 Details of specimens

Specimen	Outer tube (mm)			Inner tube (mm)			f_c'	N_t
	D_o	t_o	Mat.	D_i	t_i	Mat.	(MPa)	(kN)
S50-H	50.9	3.07	SS	N/A	N/A	N/A	N/A	200
S101-H	101.9	2.79	SS	N/A	N/A	N/A	N/A	250
S114-H	114.1	2.79	SS	N/A	N/A	N/A	N/A	332
S165-H	168.4	3.22	SS	N/A	N/A	N/A	N/A	536
C50-H	50.5	2.81	CFRP	N/A	N/A	N/A	N/A	83
C101-H	99.9	2.81	CFRP	N/A	N/A	N/A	N/A	145
C114-H	114.6	2.75	CFRP	N/A	N/A	N/A	N/A	172
C165-H	158.1	2.79	CFRP	N/A	N/A	N/A	N/A	203
B50-H	50.0	2.71	BFRP	N/A	N/A	N/A	N/A	51
B101-H	100.0	2.92	BFRP	N/A	N/A	N/A	N/A	94
B114-H	114.5	2.78	BFRP	N/A	N/A	N/A	N/A	88
B165-H	157.7	2.71	BFRP	N/A	N/A	N/A	N/A	124
S50-C	50.9	3.07	SS	N/A	N/A	N/A	35.8	235[a]
S101-C	101.9	2.79	SS	N/A	N/A	N/A	35.8	570[a]
S114-C	114.1	2.79	SS	N/A	N/A	N/A	35.8	766[a]
S165-C	168.4	3.22	SS	N/A	N/A	N/A	35.8	1449[a]
C50-C	50.5	2.81	CFRP	N/A	N/A	N/A	35.8	388
C101-C	99.9	2.81	CFRP	N/A	N/A	N/A	35.8	1131
C114-C	114.6	2.75	CFRP	N/A	N/A	N/A	35.8	1416
C165-C	158.1	2.79	CFRP	N/A	N/A	N/A	35.8	2372
B50-C	50.0	2.71	BFRP	N/A	N/A	N/A	32.8	259
B101-C	100.0	2.92	BFRP	N/A	N/A	N/A	32.8	656
B114-C	114.5	2.78	BFRP	N/A	N/A	N/A	32.8	825
B165-C	157.7	2.71	BFRP	N/A	N/A	N/A	32.8	1345
S114-S50-C	114.1	2.79	SS	50.9	3.07	SS	39.4	852[a]
S165-S101-C	168.4	3.22	SS	101.9	2.79	SS	39.4	1314[a]
S114-C50-C	114.1	2.79	SS	50.5	2.81	CFRP	39.4	735[a]
S165-C101-C	168.4	3.22	SS	99.9	2.81	CFRP	39.4	1271[a]
C114-S50-C	114.6	2.75	CFRP	50.9	3.07	SS	39.4	1375
C165-S101-C	158.1	2.79	CFRP	101.9	2.79	SS	39.4	1698
C114-C50-C	114.6	2.75	CFRP	50.5	2.81	CFRP	39.4	1175
C165-C101-C	158.1	2.79	CFRP	99.9	2.81	CFRP	39.4	1219
S114-B50-C	114.1	2.79	SS	50.0	2.71	BFRP	32.8	676[a]
S165-B101-C	168.4	3.22	SS	100.0	2.92	BFRP	32.8	1145[a]
B114-S50-C	114.5	2.78	BFRP	50.9	3.07	SS	32.8	884
B165-S101-C	157.7	2.71	BFRP	101.9	2.79	SS	32.8	1053
B114-B50-C	114.5	2.78	BFRP	50.0	2.71	BFRP	32.8	651
B165-B101-C	157.7	2.71	BFRP	100.0	2.92	BFRP	32.8	703

[a]: The load corresponding to 5% axial strain was adopted as N_t

Table 2 Material properties of stainless steel

Tube size	$f_{0.2}$ (MPa)	f_u (MPa)
S50	228.2	562.1
S101	225.7	656.4
S114	280.7	617.8
S165	281.1	615.8
Mean	253.9	613.0
COV	0.11	0.05

Table 3 Material properties of CFRP, BFRP and GFRP

FRP type	Tube size	Longitudinal direction				Hoop direction			
		f_{ul} (MPa)	ε_{ul}	E_l (GPa)	ν_l [a]	f_{uh} (MPa)	ε_{uh}	E_h (GPa)	ν_h
CFRP	C50	244.7	0.0089	40.6	0.25	631.4	0.0096	75.6	0.51
	C101	240.5	0.0092	37.8	0.27	581.8	0.0102	65.1	0.51
	C114	230.3	0.0086	39.6	0.27	562.6	0.0103	63.6	N/A
	C165	256.0	0.0084	44.0	0.27	595.5	0.0099	62.5	0.53
	Mean	242.9	0.0088	40.5	0.26	592.8	0.0100	66.7	0.52
	COV	0.044	0.040	0.064	0.038	0.049	0.032	0.090	0.022
BFRP	B50	116.0	0.0129	13.7	0.28	334.6	0.0145	22.8	0.30
	B101	128.3	0.0154	12.4	0.30	329.4	0.0147	24.1	N/A
	B114	126.0	0.0138	12.1	0.29	340.6	0.0158	25.8	N/A
	B165	123.1	0.0142	12.7	0.29	319.6	0.0144	24.4	0.30
	Mean	124.0	0.0142	12.7	0.29	331.1	0.0149	24.3	0.30
	COV	0.043	0.074	0.055	0.028	0.027	0.043	0.051	0.000
GFRP[b]	Mean	217.6	0.0190	20.1	0.32	308.8	0.0139	25.2	N/A
	COV	0.11	0.31	0.10	0.08	0.16	0.07	0.04	N/A

[a]: Poisson's ratio in longitudinal direction was obtained from stress-strain curves of hollow sections.
[b]: From Li et al. [18]

Table 4 Test results of SS hollow sections

Specimen	D_o/t_o	$f_{0.2}$ (MPa)	σ_t (MPa)	$\sigma_t/f_{0.2}$	ε_t	
					From LVDT	From strain gauge
S50-H	16.6	228.2	433.3	1.90	0.1081	0.0722
S101-H	36.6	225.7	288.1	1.28	0.0306	0.0295
S114-H	40.9	280.7	340.5	1.21	0.0241	0.0179
S165-H	52.3	281.1	320.3	1.14	0.0156	0.0124

Table 5 Test results of CFRP and BFRP hollow sections

Specimen	D_o/t_o	Material properties			σ_t (MPa)	σ_t/f_{ul}	σ_{res} (MPa)	ε_t		Stiffness (GPa)	
		f_{ul} (MPa)	ε_{ul}	E_l (GPa)				From LVDT	From strain gauge	From LVDT	From strain gauge
C50-H	18.0	242.9	0.0088	40.5	197.4	0.81	134.5	0.0071	0.0051	27.9	39.2
C101-H	35.6	242.9	0.0088	40.5	169.0	0.70	112.9	0.0078	0.0045	30.2	38.1
C114-H	41.7	242.9	0.0088	40.5	178.4	0.73	30.5	0.0074	0.0045	32.0	39.9
C165-H	56.7	242.9	0.0088	40.5	149.6	0.62	76.1	0.0043	0.0034	35.4	42.9
Mean							88.5			31.4	40.0
COV							0.515			0.101	0.051
B50-H	18.5	124.0	0.0142	12.7	126.5	1.02	43.2	0.0074	0.0031	16.8	24.2
B101-H	34.3	124.0	0.0142	12.7	105.8	0.85	58.8	0.0053	0.0023	20.6	25.7
B114-H	41.2	124.0	0.0142	12.7	90.2	0.73	69.5	0.0051	0.0027	19.6	22.6
B165-H	58.2	124.0	0.0142	12.7	94.0	0.76	65.5	0.0078	0.0026	18.1	23.0
Mean							59.3			18.8	23.9
COV							0.195			0.089	0.058

Table 6 First buckling strain of CFRP and BFRP tubes

Specimen	From LVDT						From strain gauge		
	Inner	Hollow	Inner/ Hollow	Outer	Hollow	Outer / Hollow	Outer	Hollow	Outer / Hollow
C50-C	N/A	N/A	N/A	0.010	0.007	1.35	0.009	0.005	1.69
C101-C	N/A	N/A	N/A	0.011	0.008	1.48	0.008	0.004	1.83
C114-C	N/A	N/A	N/A	0.009	0.007	1.25	0.007	0.004	1.50
C165-C	N/A	N/A	N/A	0.012	0.004	2.72	0.007	0.003	2.22
S114-C50-C	0.010	0.007	1.43	N/A	N/A	N/A	N/A	N/A	N/A
S165-C101-C	0.011	0.008	1.41	N/A	N/A	N/A	N/A	N/A	N/A
C114-S50-C	N/A	N/A	N/A	0.008	0.007	1.13	0.007	0.004	1.52
C165-S101-C	N/A	N/A	N/A	0.010	0.004	2.30	0.006	0.003	1.65
C114-C50-C	N/A	N/A	N/A	0.009	0.007	1.17	0.006	0.004	1.41
C165-C101-C	0.011	0.008	1.37	0.008	0.004	1.77	0.006	0.003	1.80
Mean	0.011			0.010			0.007		
B50-C	N/A	N/A	N/A	0.014	0.007	1.87	0.009	0.003	2.90
B101-C	N/A	N/A	N/A	0.008	0.005	1.59	0.007	0.002	3.22
B114-C	N/A	N/A	N/A	0.010	0.005	1.96	0.008	0.003	2.93
B165-C	N/A	N/A	N/A	0.010	0.008	1.34	0.008	0.003	2.93
S114-B50-C	0.007	0.007	1.00	N/A	N/A	N/A	N/A	N/A	N/A
S165-B101-C	0.008	0.005	1.42	N/A	N/A	N/A	N/A	N/A	N/A
B114-S50-C	N/A	N/A	N/A	0.010	0.005	1.94	0.008	0.003	2.91
B165-S101-C	N/A	N/A	N/A	0.011	0.008	1.35	0.008	0.003	3.21
B114-B50-C	0.008	0.007	1.05	0.009	0.005	1.80	0.006	0.003	2.39
B165-B101-C	0.006	0.005	1.20	0.011	0.008	1.36	0.007	0.003	2.76
Mean	0.007			0.010			0.008		

Table 7 Ultimate axial strain (from LVDTs) and ultimate hoop strain corresponding to ultimate capacity

Specimen	Axial direction		Hoop direction	
	ε_{tl}	ε_{ul}	ε_{th}	ε_{uh}
C50-C	0.058	0.009	N/A	0.010
C101-C	0.051		0.011	
C114-C	0.051		0.013	
C165-C	0.046		0.012	
C114-S50-C	0.052		0.012	
C165-S101-C	0.058		0.015	
C114-C50-C	0.056		0.014	
C165-C101-C [a]	0.028		0.007	
B50-C	0.053	0.014	N/A	0.015
B101-C	0.038		0.014	
B114-C	0.032		0.014	
B165-C	0.034		0.018	
B114-S50-C	0.040		0.016	
B165-S101-C	0.035		0.016	
B114-B50-C [a]	0.034		0.011	
B165-B101-C [a]	0.024		0.007	

[a]: No outer tube rupture

Table 8 Comparison between the experimental capacity and estimated capacity of fully SWSSC-filled SS tubes

Data source	Specimen	$f_{0.2}$ (MPa)	f_c' (MPa)	ξ	f_{scy} (MPa)	N_t (kN)	N_p (kN)	N_p/N_t
This paper	S50-C	228.2	35.8	1.87	134.6	235	274	1.16
	S101-C	225.7	35.8	0.75	78.4	570	640	1.12
	S114-C	280.7	35.8	0.83	82.3	766	841	1.10
	S165-C	281.1	35.8	0.64	72.7	1449	1620	1.12
Li et al. [18]	S101-C	324.4	31.4	1.26	91.2	729	734	1.01
	S114-C	270.3	31.4	0.94	77.2	800	786	0.98
	S165-C	280.1	31.4	0.71	66.9	1522	1487	0.98
Mean								1.07
COV								0.070

Table 9 Comparison between experimental capacity and estimated capacity of SWSSC-filled double-skin tubes (SS as the outer tube)

Data source	Specimen	f_{yo} (MPa)	f_{yi} (MPa)	f_c' (MPa)	ξ	χ	f_{scy} (MPa)	N_t (kN)	N_p (kN)	N_p/N_t
This paper	S114-S50-C	280.7	395.1	39.4	0.75	0.45	90.8	852	925	1.09
	S165-S101-C	281.1	441.0	39.4	0.58	0.61	85.4	1314	1589	1.21
	S114-C50-C	280.7	88.5	39.4	0.75	0.44	90.7	735	782	1.06
	S165-C101-C	281.1	88.5	39.4	0.58	0.59	84.9	1271	1301	1.02
	S114-B50-C	280.7	59.3	32.8	0.90	0.44	83.2	676	711	1.05
	S165-B101-C	281.1	59.3	32.8	0.70	0.59	77.7	1145	1173	1.02
Li et al. [18]	S114-S50-C	270.3	462.5	31.4	0.93	0.42	80.6	909	864	0.95
	S165-S101-C	280.1	485.8	31.4	0.72	0.60	76.1	1409	1491	1.06
	S114-G50-C	270.3	113.6	31.4	0.96	0.45	82.7	799	731	0.91
	S165-G101-C	280.1	53.9	31.4	0.72	0.60	76.0	1167	1143	0.98
Mean										1.04
COV										0.079

Table 10 Comparison between experimental capacity and estimated capacity of fully SWSSC-filled FRP tubes

Data source	Specimen	f_{ul} (MPa)	f_{uh} (MPa)	f_c' (MPa)	f_l (MPa)	f_{un} (MPa)	N_t (kN)	N_p (kN)	N_p/N_t
This paper	C50-C	242.9	592.8	35.8	66.0	214.3	388	375	0.97
	C101-C	242.9	592.8	35.8	33.3	128.1	1131	940	0.83
	C114-C	242.9	592.8	35.8	28.5	115.2	1416	1122	0.79
	C165-C	242.9	592.8	35.8	20.9	95.3	2372	1794	0.76
	B50-C	124.0	331.1	32.8	35.8	131.2	259	225	0.87
	B101-C	124.0	331.1	32.8	19.3	87.7	656	641	0.98
	B114-C	124.0	331.1	32.8	16.1	79.1	825	767	0.93
	B165-C	124.0	331.1	32.8	11.4	66.7	1345	1248	0.93
Li et al. [18]	G50-C	217.6	308.8	31.4	37.1	133.2	244	255	1.05
	G101-C	217.6	308.8	31.4	19.3	86.1	670	653	0.98
	G114-C	217.6	308.8	31.4	16.8	79.4	813	802	0.99
	G165-C	217.6	308.8	31.4	12.3	67.5	1336	1296	0.97
Mean									0.92
COV									0.097

Table 11 Comparison between experimental capacity and estimated capacity of SWSSC-filled double-skin tubes (FRP as the outer tube)

Data source	Specimen	f_{yi} (MPa)	f_{ul} (MPa)	f_{uh} (MPa)	f_c' (MPa)	f_l (MPa)	χ	N_t (kN)	N_p (kN)	N_p/N_t
This paper	C114-S50-C	395.1	242.9	592.8	39.4	28.5	0.44	1375	1101	0.80
	C165-S101-C	441.0	242.9	592.8	39.4	20.9	0.64	1698	1442	0.85
	C114-C50-C	165.7	242.9	592.8	39.4	28.5	0.44	1175	992	0.84
	C165-C101-C[a]	165.7	242.9	592.8	39.4	20.9	0.63	1219	1233	1.01
	B114-S50-C	395.1	124.0	331.1	32.8	16.1	0.44	884	788	0.89
	B165-S101-C	441.0	124.0	331.1	32.8	11.4	0.65	1053	1086	1.03
	B114-B50-C[a]	91.7	124.0	331.1	32.8	16.1	0.44	651	648	1.00
	B165-B101-C[a]	91.7	124.0	331.1	32.8	11.4	0.63	703	805	1.14
Li et al. [18]	G114-S50-C	462.5	217.6	308.8	31.4	15.6	0.42	872	815	0.93
	G165-S101-C	485.8	217.6	308.8	31.4	11.4	0.64	1301	1160	0.89
	G114-G50-C	164.6	217.6	308.8	31.4	15.7	0.45	795	688	0.87
	G165-G101-C	135.8	217.6	308.8	31.4	12.2	0.63	880	893	1.01
Mean										0.94
COV										0.106

[a]: No tube rupture